NIFSにおける NBI装置開発

津守　克嘉、NIFS NBIグループ

第16回QUEST研究会～核融合技術の進展と球状トカマク研究
九州大学 応用力学研究所、3 and 4 October 2019

Outline

- Negative-Ion Based NBI for LHD
- Plasma and Beam Uniformity
- High Performance Accelerator
- Beamlet Monitoring
- Physics Study of Source Plasmas and Beams
- Injection from Hydrogen to Deuterium Beams
- Summary

Negative-Ion Based NBI for LHD

LHD NBI

1. Profile measurement of T_i and E_r (CXRS)
   - The beam energy of tangential-NBI was too high for CXRS meas.
2. Ion heating with NBI
   - Electron heating is dominant with tangential high-energy NB injectors.
     Ion heating rate at T_e=*4 keV*:
     - ✓ Injection energy of 180 keV → 40%
     - ✓ Injection energy of 40 keV → 80%
3. D beam injection
   - BL4: max 40 keV (for H)
     [max 60 keV (for D)]
   - BL5: max 60 keV (for H)
     max 80 keV (for D)
4. Confinement study of perpendicular injected high-energy particles
   - Normalized Larmour-radius of 40keV Hydorgenic ions at 1.5T LHD-configuration is almost comparable to those of a-particles in ITER and/or FFHR-2m2

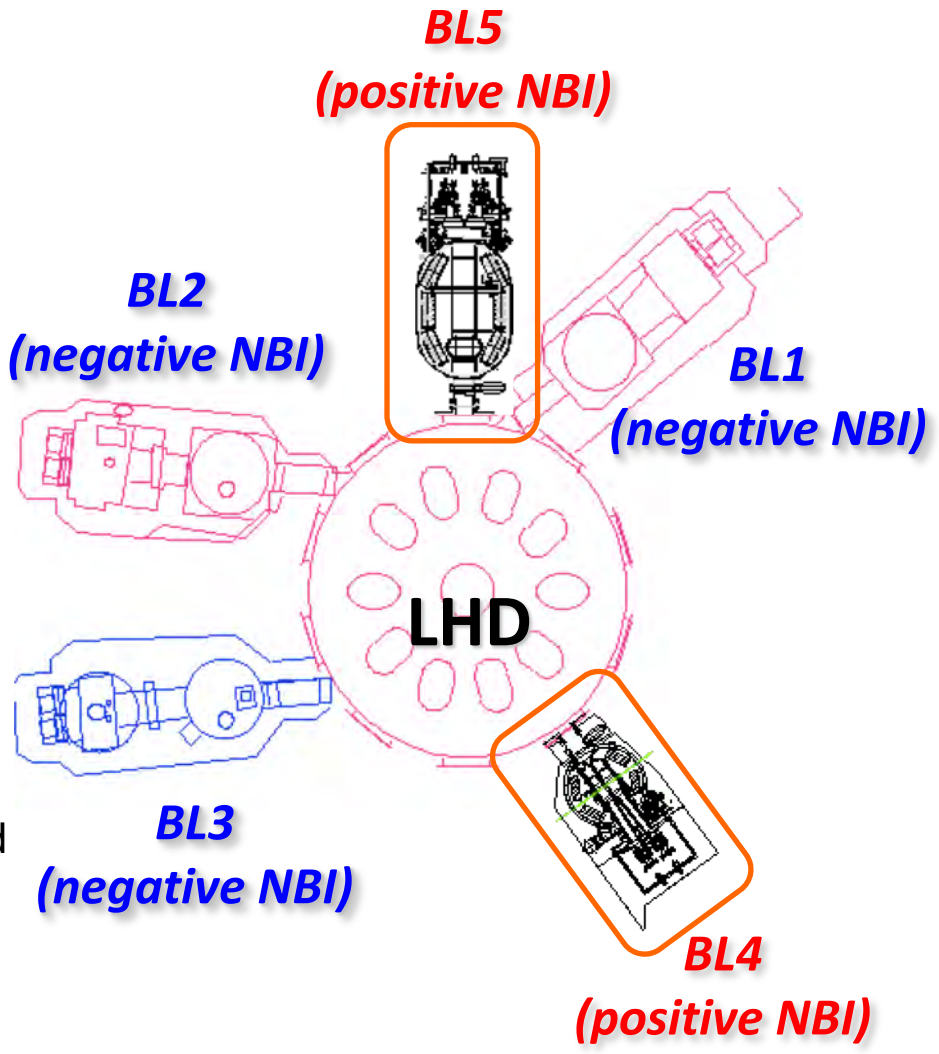

Structure of N-NBI in LHD

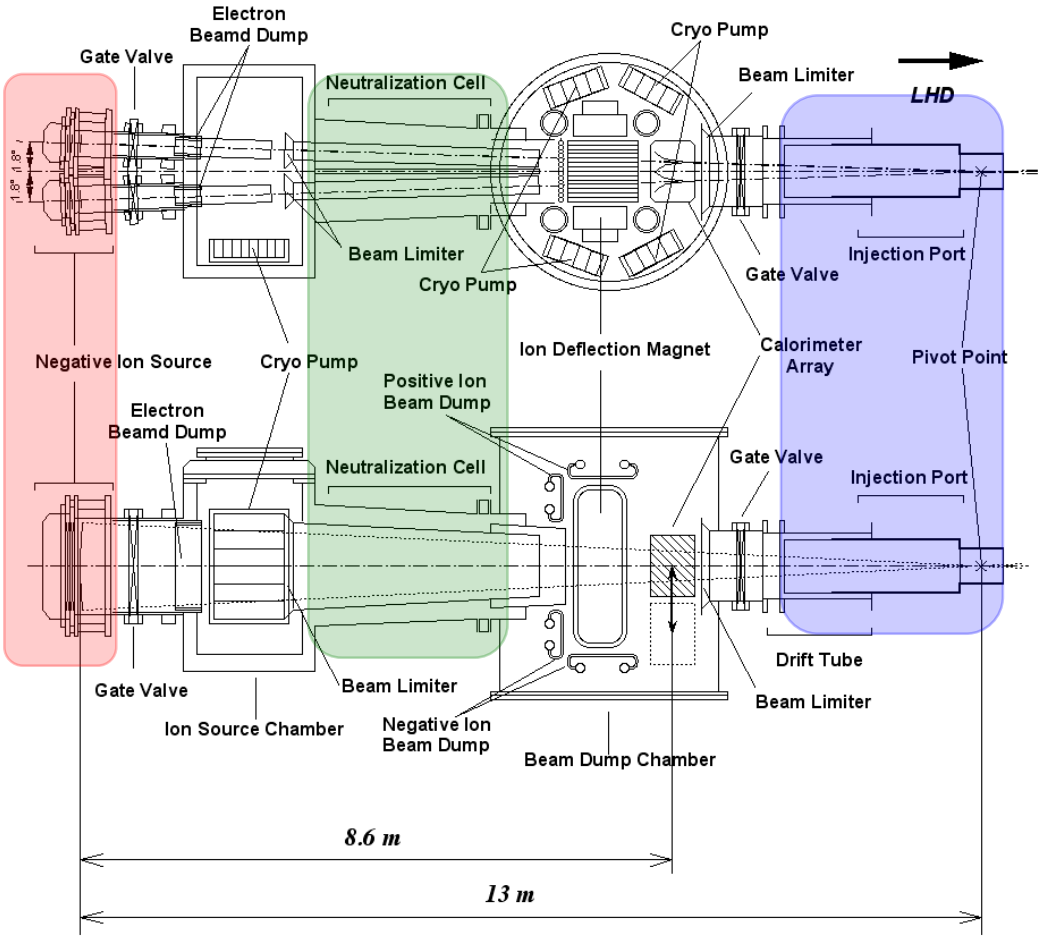

- Hydrogen beam injection with 180 keV-5 MW / injector (2 ion sources).
- Length of gas-neutralizing cell : 5 m
- Focal length of the ion source is 13 m, and pivot point of two ion sources locates 15.4 m in the horizontal direction.
- Injection port is ~3 m long, and the narrowest part is ~0.5 m in diameter with the length of ~0.7 m.

Hydrogen/Deuterium Negative Ion Source

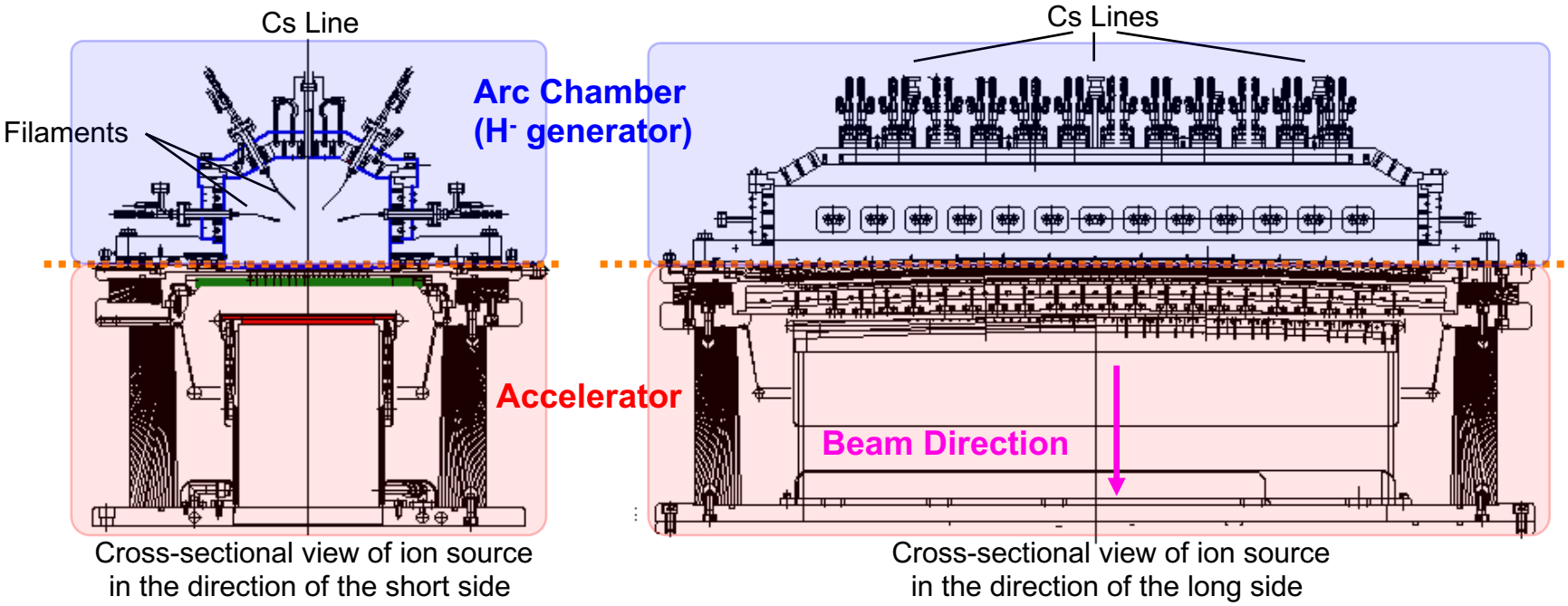

- Multi-cusp source with external magnetic filter
- Plasma production : Filament arc discharges
- Cs vapor is seeded to enhance H^- production
- Inner dimensions : 1400 mm (H) x 350 mm (W) x 230 mm (D)
- H^- beam : Single stage acceleration
- Beam extraction area : 1250 mm (H) x 250 (W)

Issues to be achieved

Stable beam injection

Sufficient H^-/D^- production

- High H^-/D^- current to discharge power
  → stability for long duration
- Plasma uniformity
- Effective and stable Cs operation

Effective beam acceleration

- Optimization for beam optics of H^-/D^- beams
  → less accelerator breakdown
- Beam uniformity
- High performance accelerator
  → High port through rate with high power beams

Physics study of ion-source plasma and beam

- Physics of negative ion plasma
- Negative ion production
- Extraction mechanism of negative ions
- Meniscus formation

Plasma and Beam Uniformity

Improvement of Arc Efficiency

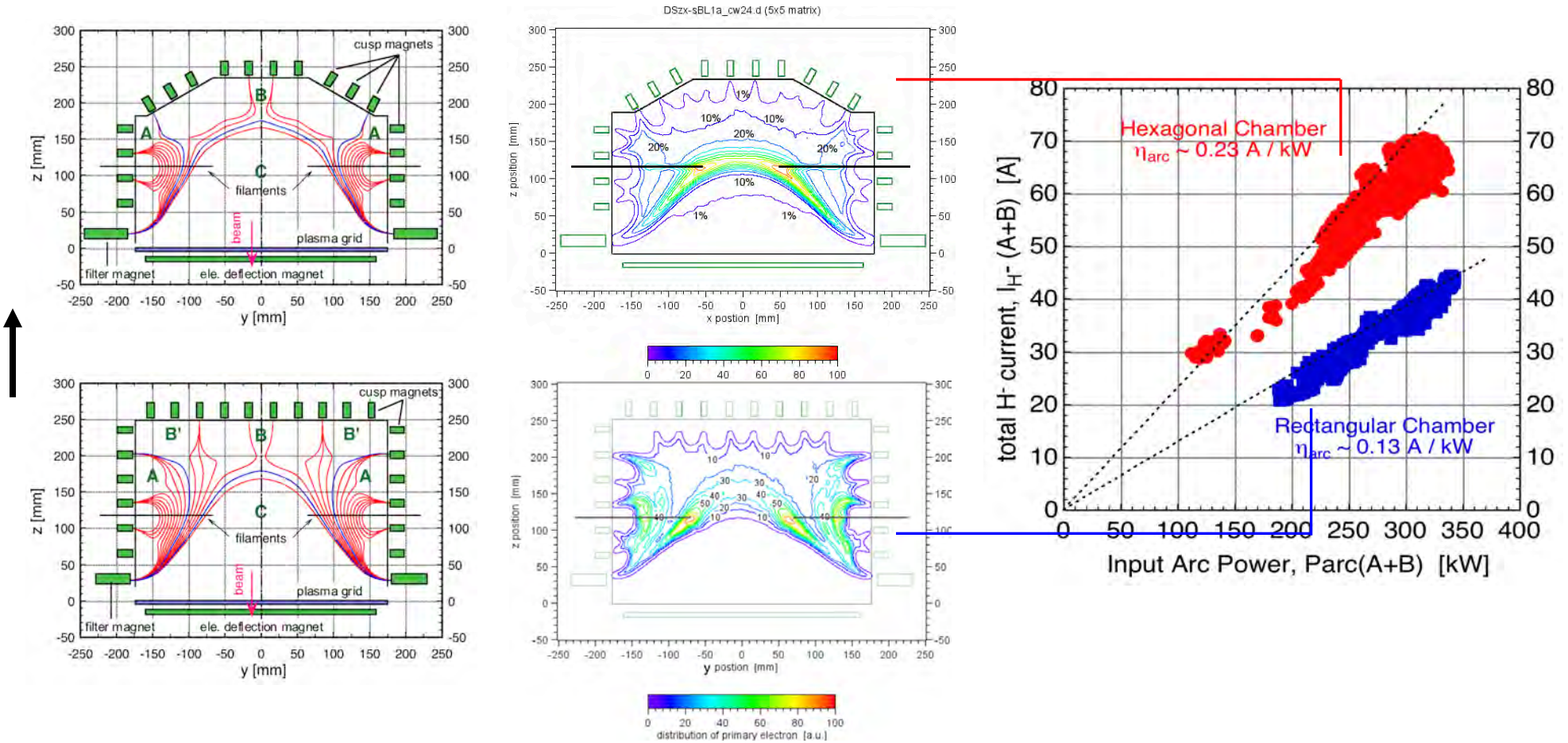

- Better electron confinement → higher atom and proton densities
- The distribution of primary electrons is better for H^- production in the optimized configuration of cusp magnets.
- The arc efficiency: 0.13 A/kW → 0.23 A/kW

Electron Drift inside Arc Chamber

Arc plasma is shift on the one long side of due to the one directional electron drift caused by the magnetic field inside the arc chamber.

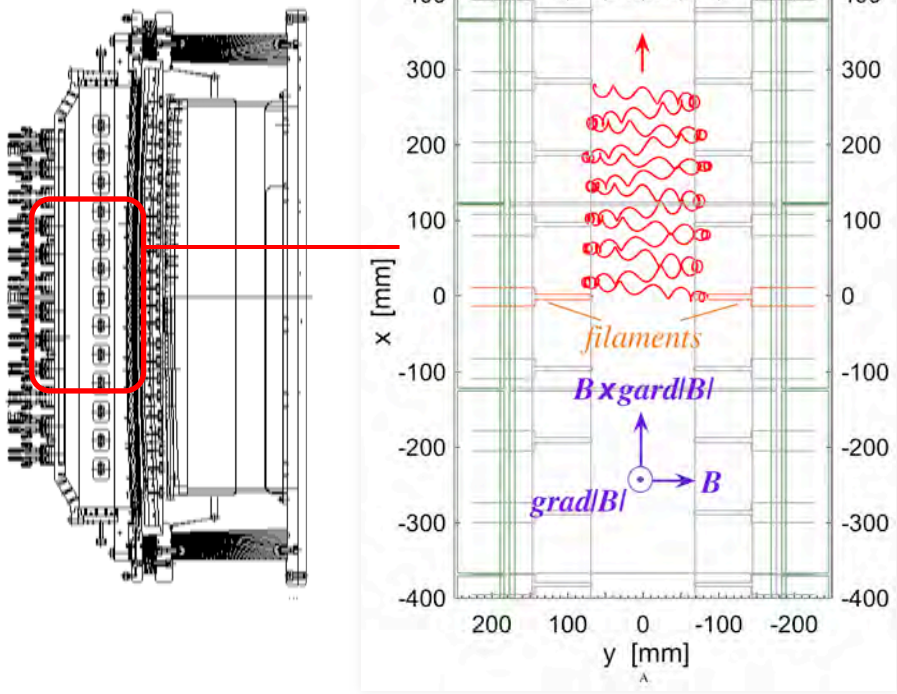

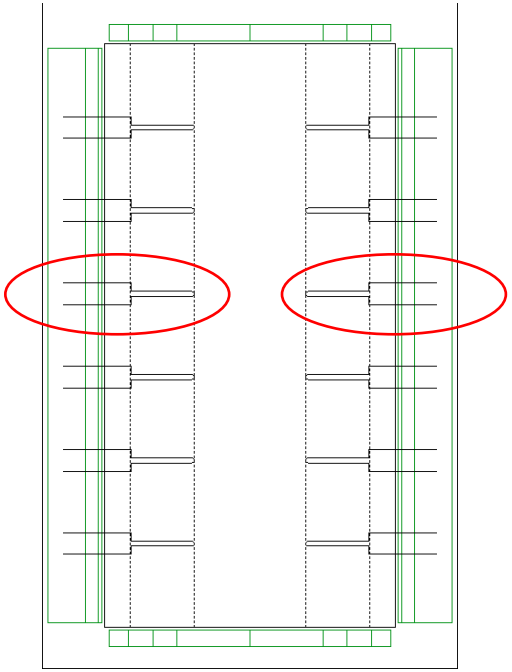

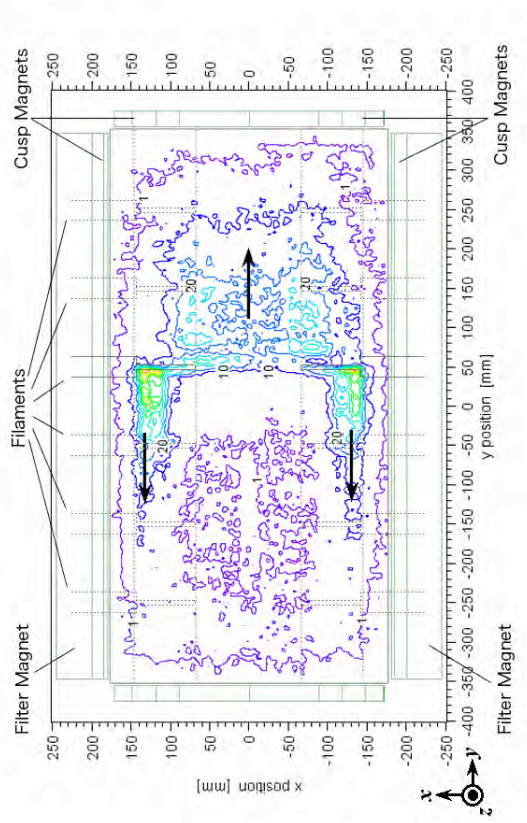

Plasma Uniformity

- In order to adjust the plasma shift, the filament and arc power supplies are separated into 12 modules, and each modules are connected a pair of filaments at ion source.
- Using the separated power supplies, distribution of arc-plasma density can be controlled considerably uniform.

Beamline 3

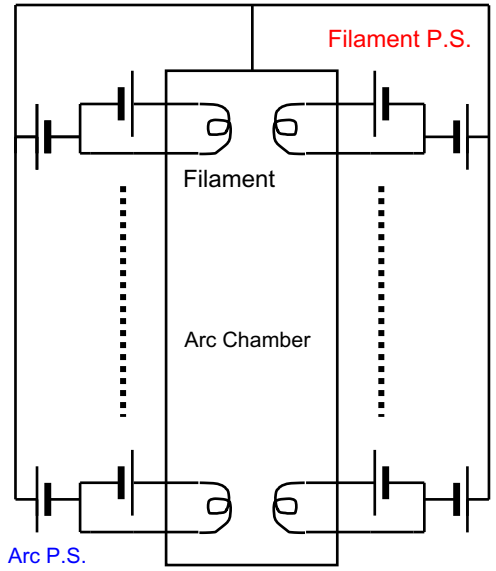

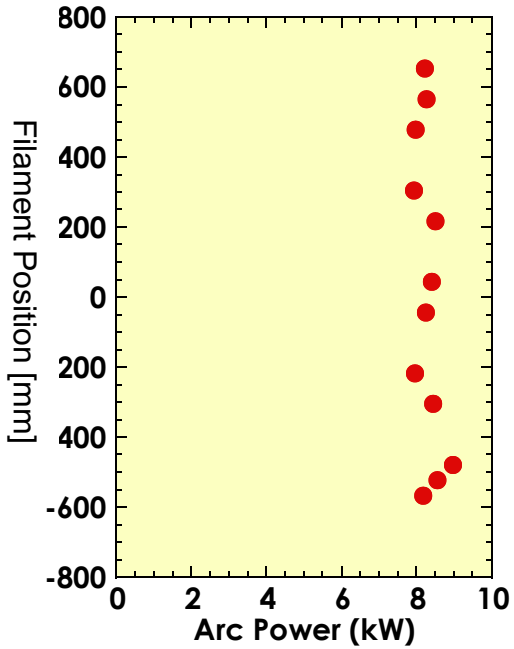

Beam Uniformity 1

- Extracted beam distribution is controlled by adjusting the arc plasma distribution.
- The beam profile is monitored at 2.2 m downstream of the ion source by the Hα video camera and at 8.5 m downstream by the calorimeter array.

Beamline 3

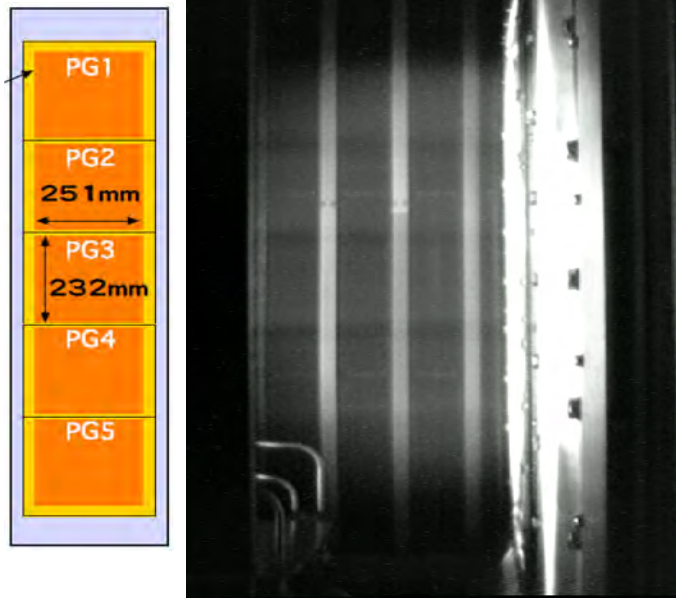

CCD view of Ha intensity 2.2m downstream

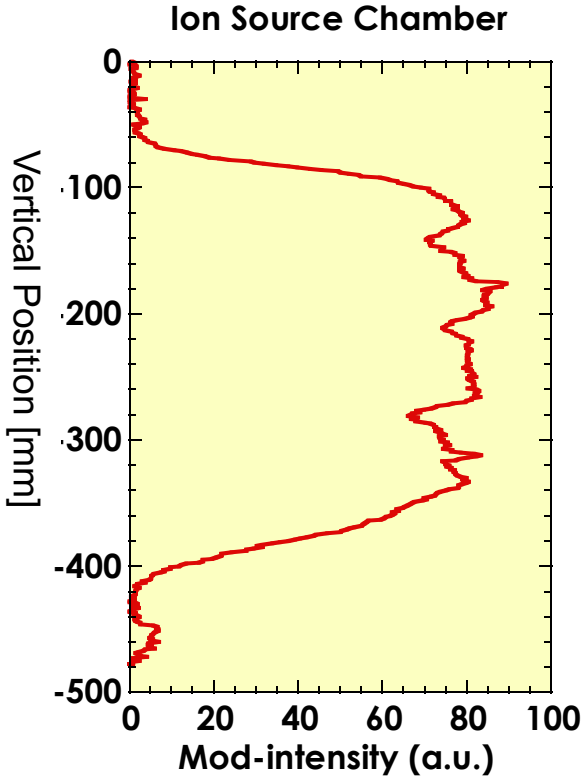

Distribution of Ha intensity 2.2m downstream

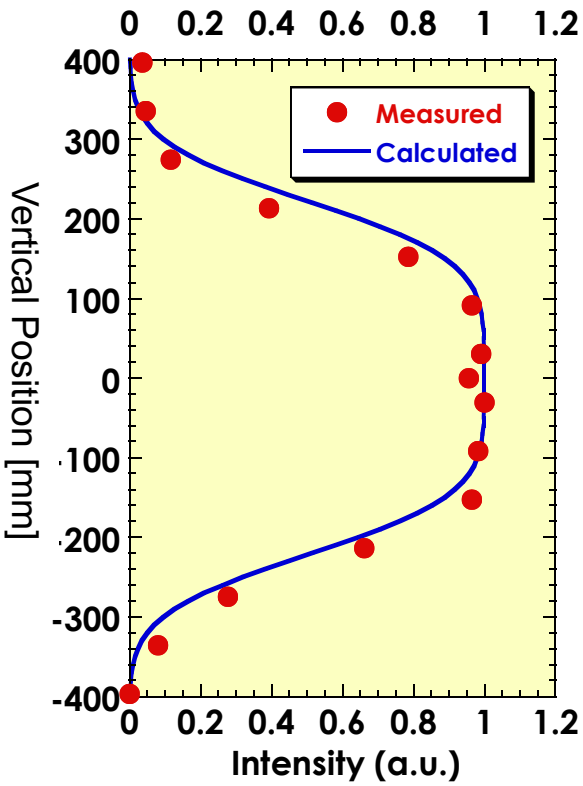

Beam profile on calorimeter 8.5m downstream

High Performance Accelerator

Highest beam heat load onto grounded grid

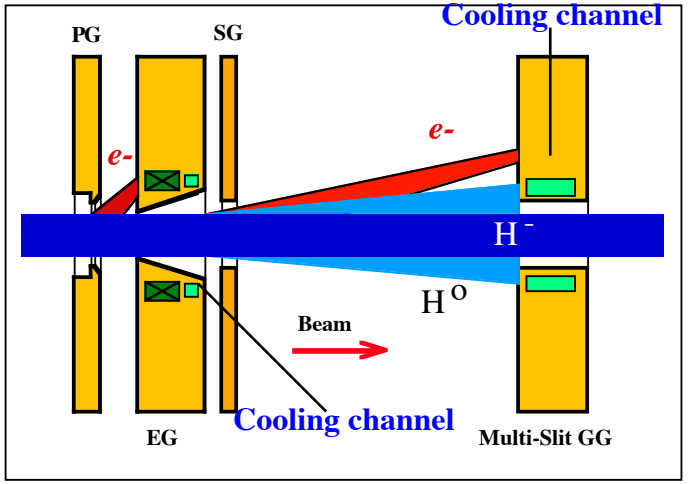

Beam heat load onto grids

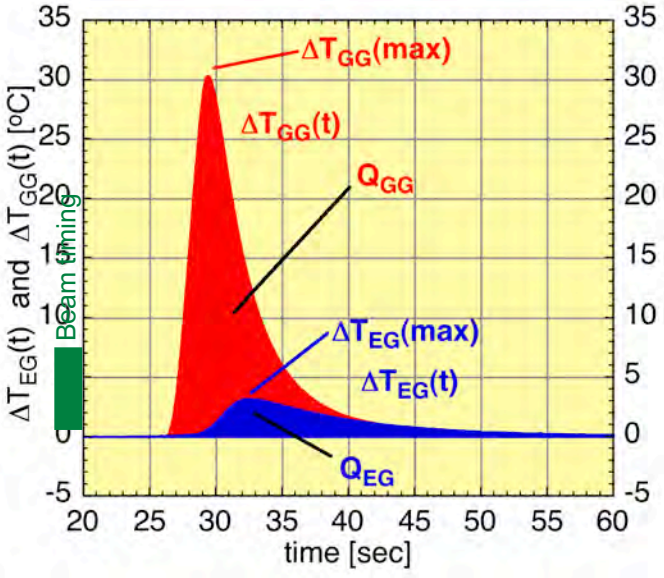

Comparison of beam heat load onto EG and GG
(Green mark denotes beam timing and duration)

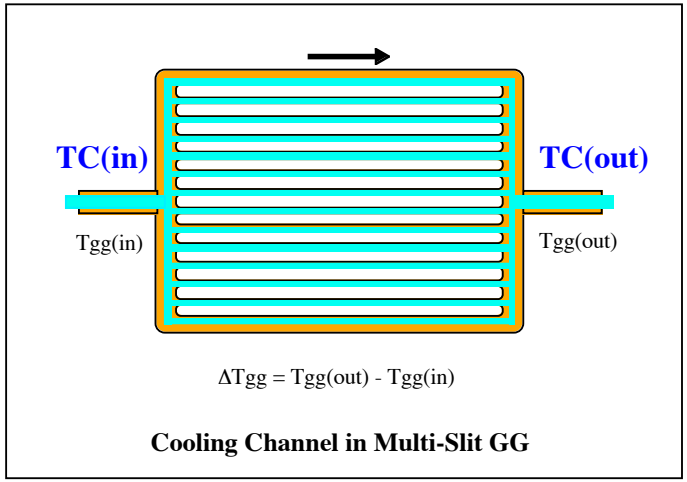

Water calorimetric to measure grid heat load

- Beam heat loads onto EG and GG were measured by means of water calorimetric technique.
- The measurement shows that heat load onto GG is much larger than that onto EG.

Multi-hole to multi-slot grounded grid

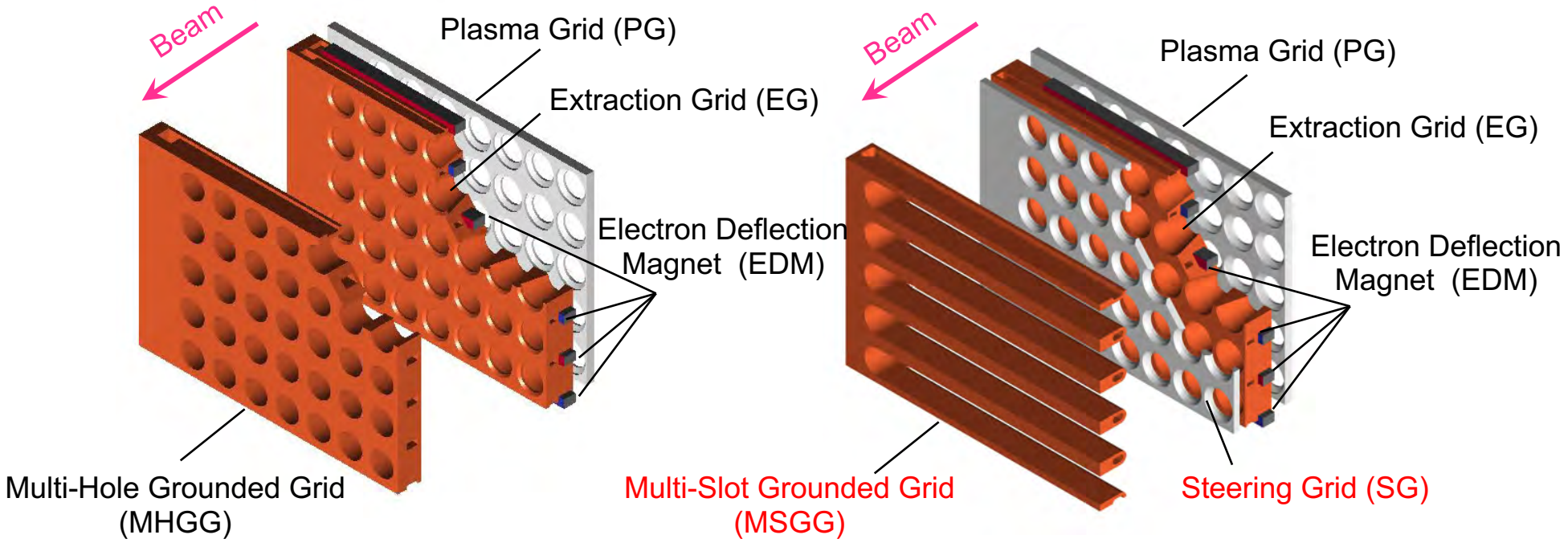

Beam accelerator with multi-hole grounded grid

- Plasma Grid : made of Mo
- Extraction Grid : including electron deflection magnets
- Grounded Grid : Multi-aperture grid

Beam accelerator with multi-slot grounded grid

- Plasma Grid : made of Mo
- Extraction Grid : electron deflection magnets are inside
- **Steering Grid** : made of Mo
- **Grounded Grid**: Multi-slot grid

Multi-hole and multi-slot grounded grid

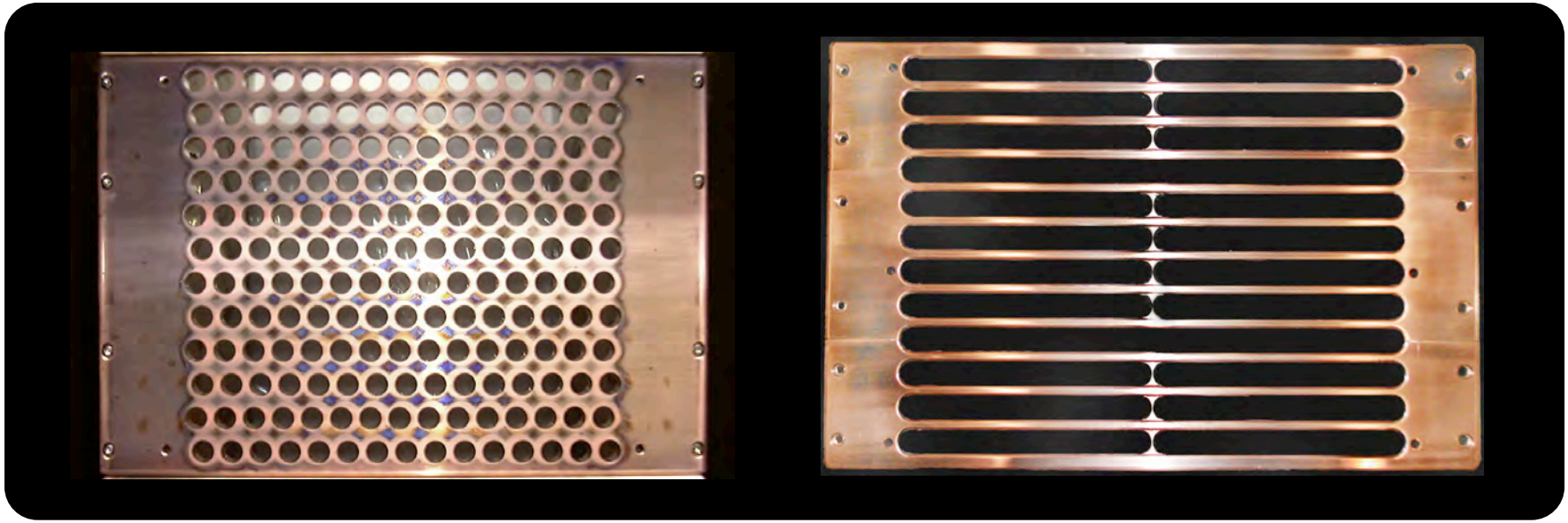

Multi-Hole Grounded Grid (MHGG)

Multi-Slot Grounded Grid (MSGG)

- Beam heat load onto the grounded grid is larger than that onto the others.
- A single slot corresponds to a single row of multi-hole.
- Beam transparency of the MSGG is twice as large as that of MHGG.
- Steering grid is added to adjust the beamlet trajectories.

Beam Heat Load on Multi-Hole and Multi-Slot Grounded Grids

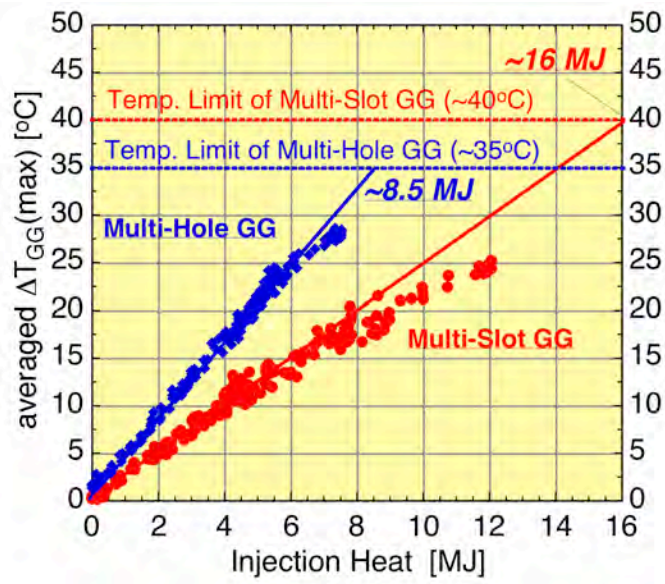

Temperature rise of multi-hole and multi-slot GGs with respect to injection heat

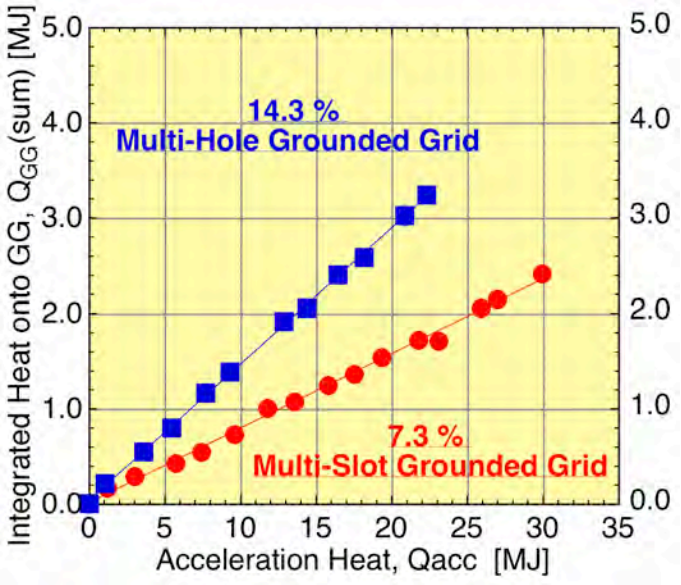

Heat load onto multi-hole and multi-slot GGs with respect to acceleration heat

- The MSGG has the heat acceptance corresponding to injection heat of ~16 MJ
- The ratios of heat load to acceleration heat onto MHGG and MSGG are 14.3 % and 7.3 %, respectively.
- The ratio on MSGG is a half value to that on MHGG. The ratio of 7.3 to 14.3 % is inverse proportional to the grid transparency.

Progress of injection power (1998 - 2004)

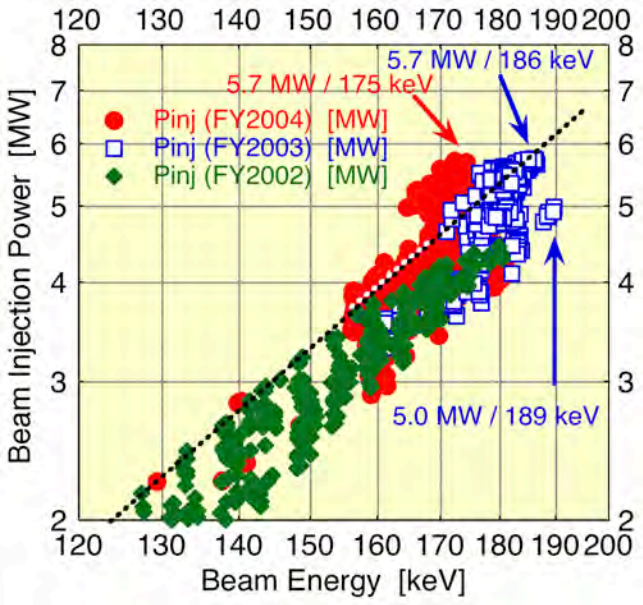

The maximum injection powers and energies obtained with MSGG from 2002 to 2004.

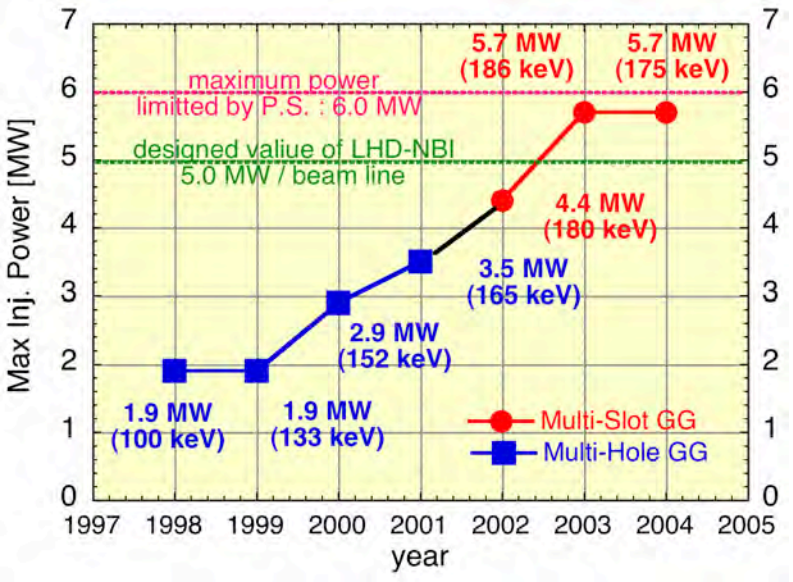

Progress of the maximum injection power by year.

- The injection power and energy increased by using the accelerator with MSGG.

FY2002 : ***4.4 MW / 180 keV / 2.0 sec***

FY2003 : ***5.7 MW / 186 keV / 1.6 sec***

5.0 MW / 189 keV / 2.0 sec

FY2004 : ***5.7 MW / 175 keV / 2.0 sec***

Trouble due to Beam Elongation

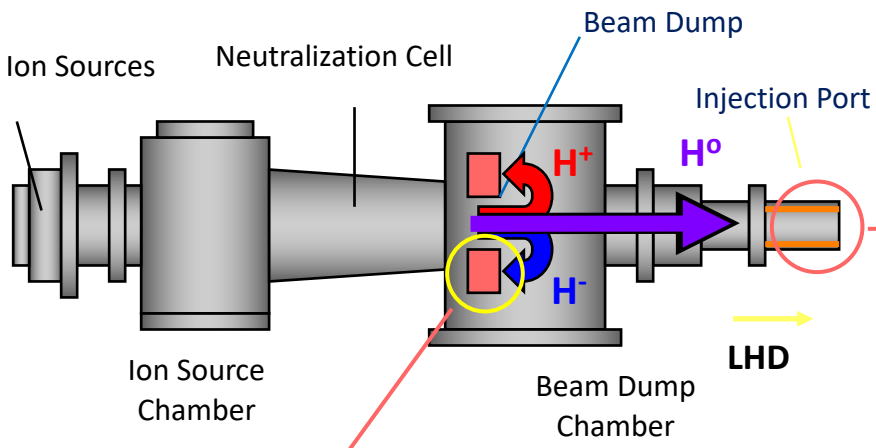

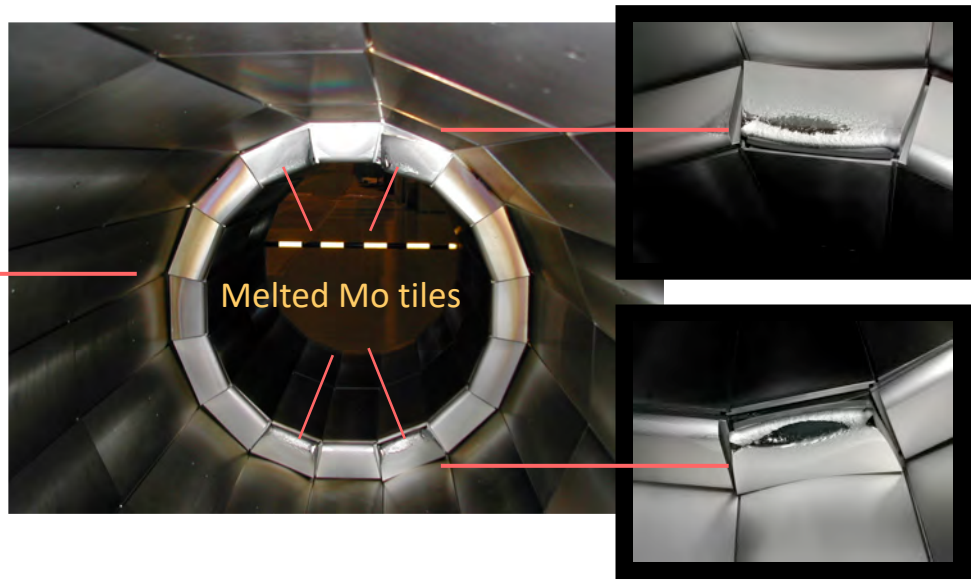

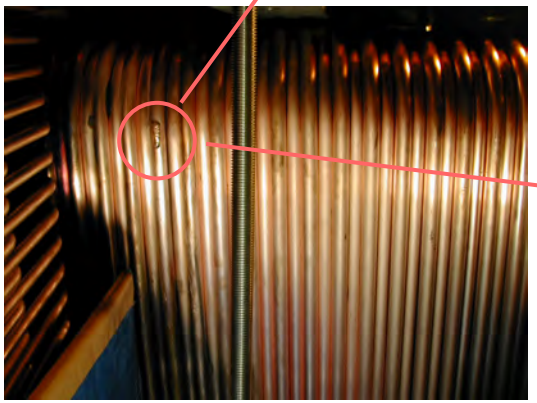

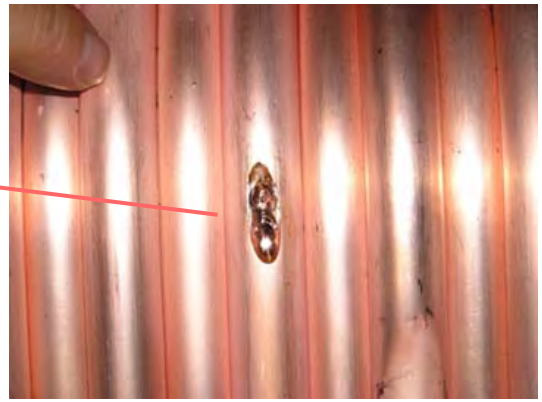

Elongated beam in one direction concentrates on some places in the beamline.

Negative beam dump and some amours protecting injection port were melted due to the beam concentration.

Bi-focal Characteristic of Multi-Slot Grid

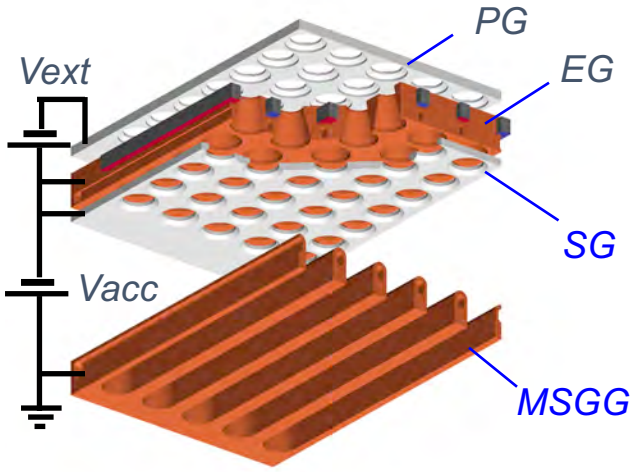

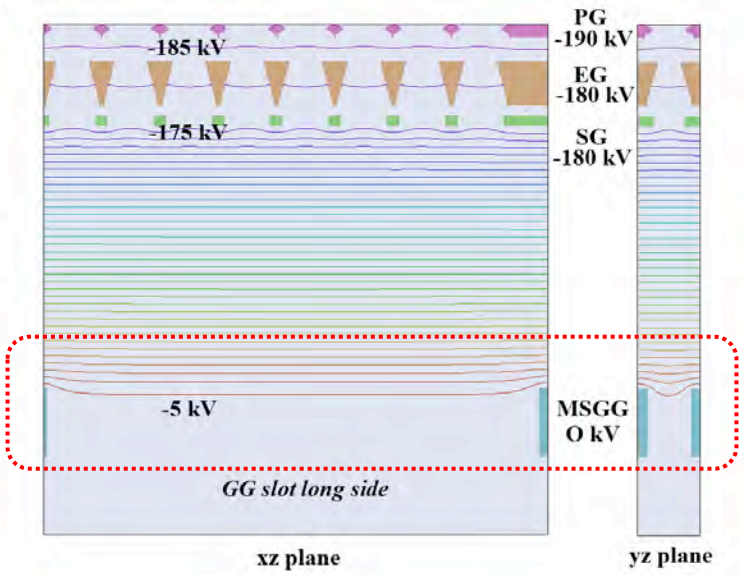

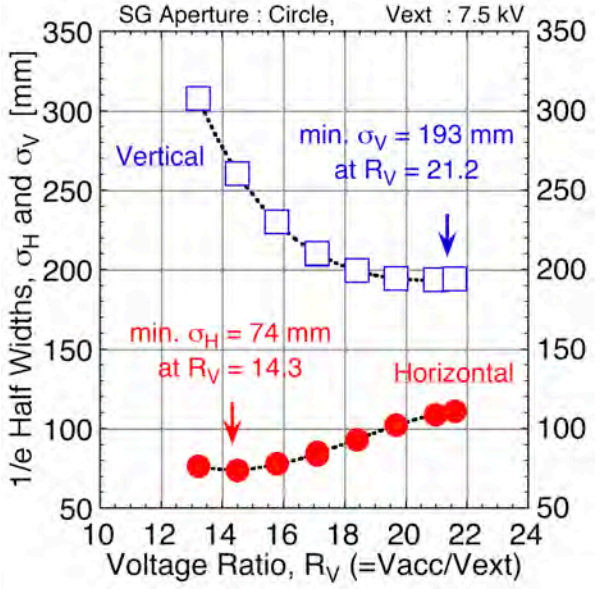

- Mismatch of symmetry
  - The SG apertures: Axial symmetric.
  - MSGG slot: Mirror symmetric.
- Defocusing effect is different along the GG-slot long and short sides.
- Consequently, the focal condition separates in both directions of parallel and perpendicular to the slot long side.

Improvement for Beam Optics

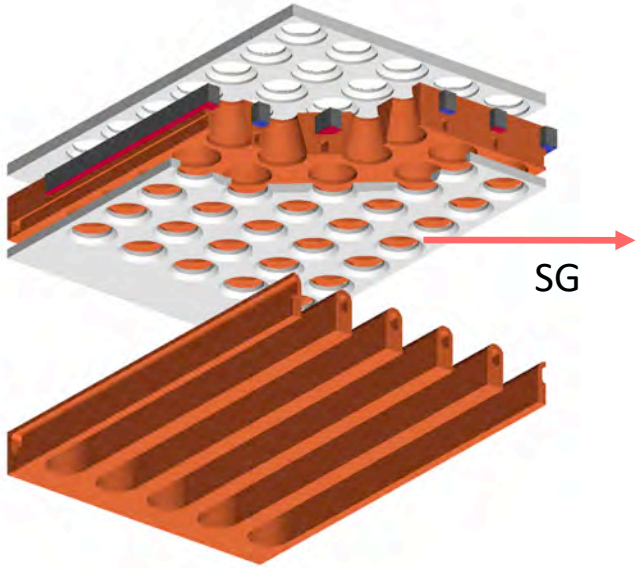

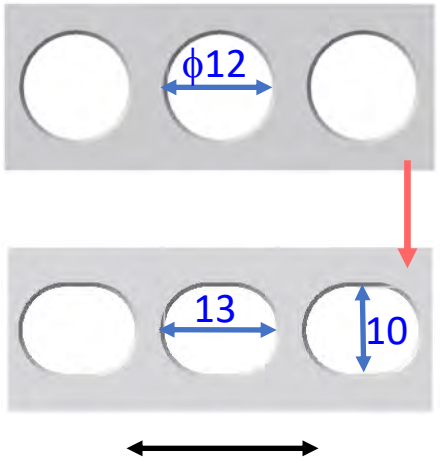

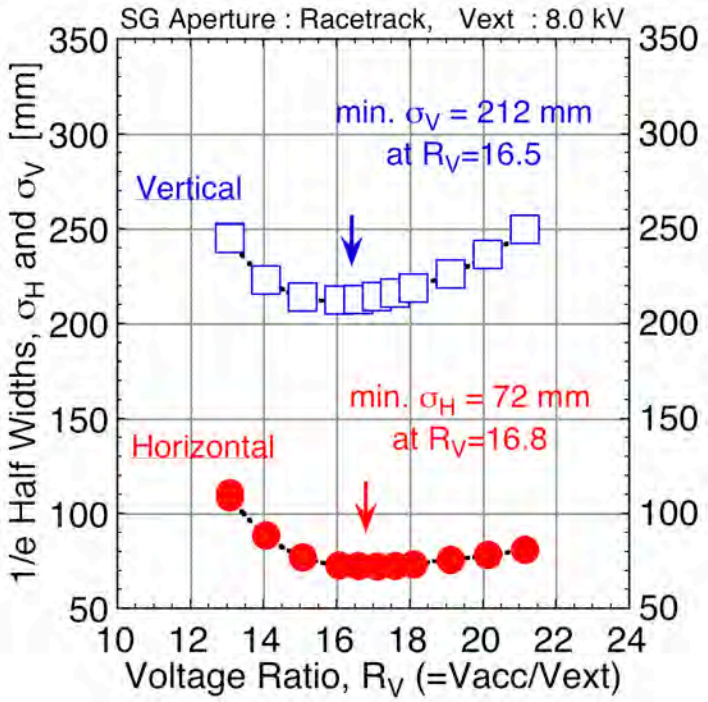

- The MSGG works one directional defocus lens. Pre-compression in the direction along the slot short side can compensate the bi-focal beam characteristic.
- Racetrack apertures are adopted to the SG, and the bi-focal condition was reduced.

Beamlet Monitoring

Beamlet Monitor

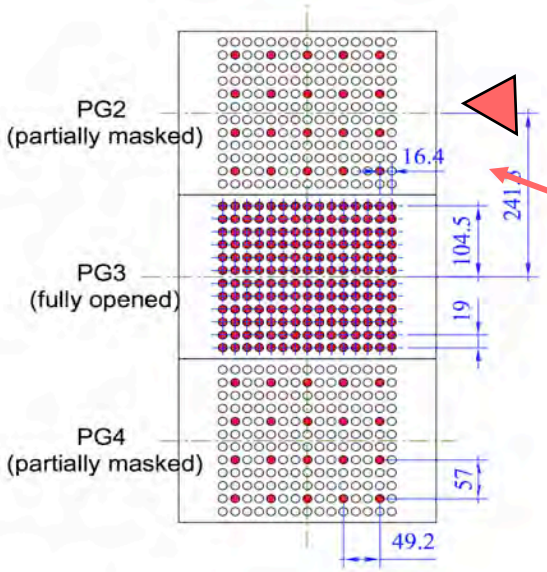

Fig. 1. Opening apertures at PG (solid red circles)

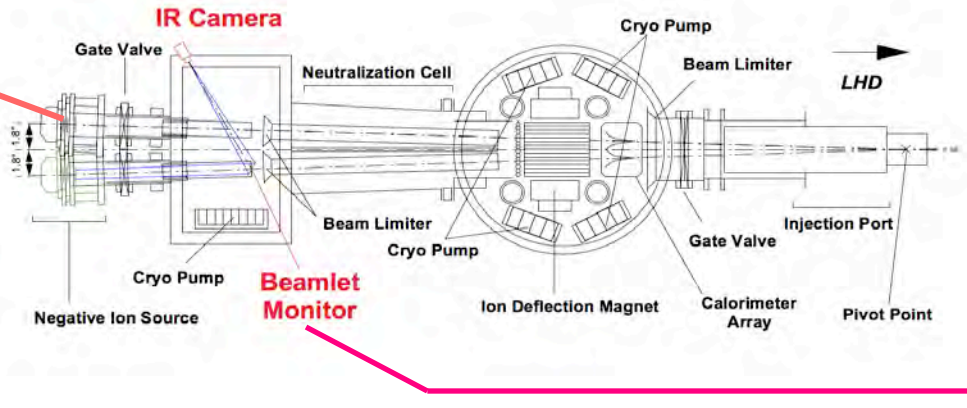

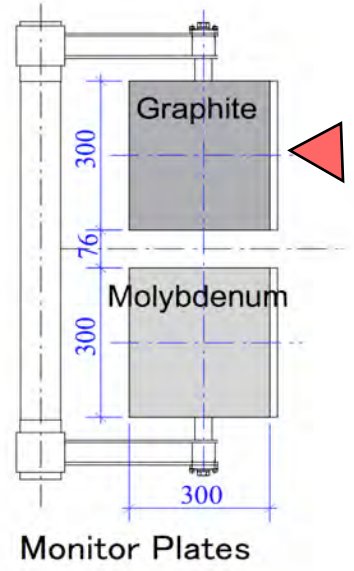

Fig. 2. NBI-beamline and beamlet monitor

- Beamlet monitor plates made of graphite is installed in the beamline, and beam-carrying heat is observed as temperature rise
- Temperature distribution is monitored using an infrared camera through ZnSe viewing window.
- Beam extraction area at plasma grids (PGs) are covered by the masks, which limit the aperture pitches of 3 x 3 as shown in Fig. 1.
- Using the limiter mask, whole the beamlet profile is possible to observe without overlapping the beamlet tail area.

Infrared Images of Beamlets

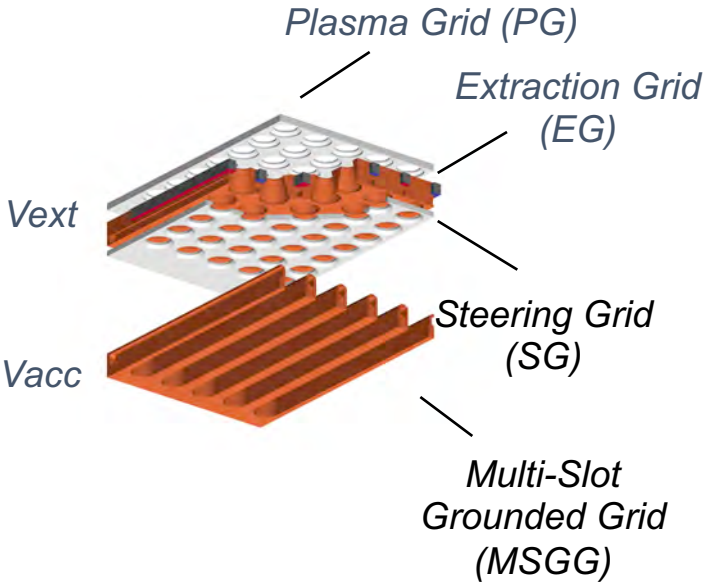

Connection of voltage power supplies
to each electrode grid
Vext : extraction voltage
Vacc : acceleration voltage

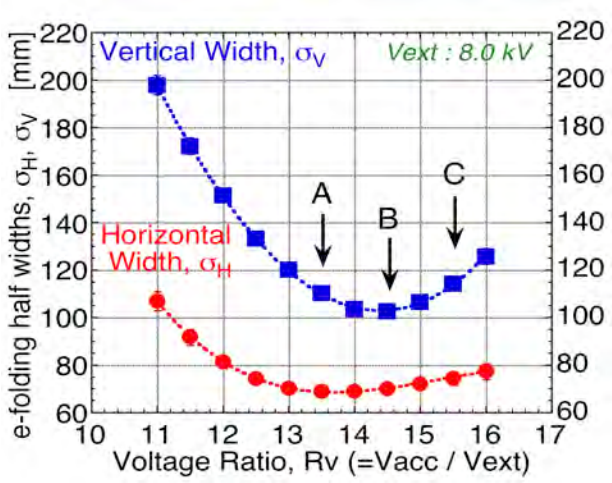

Voltage ratio (Rv=Vacc/Vext)
and global beam profile

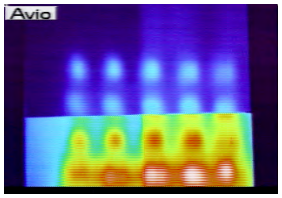

A: Rv=13.5

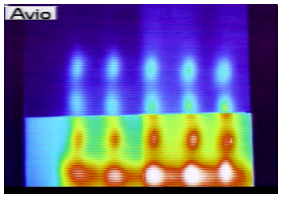

B: Rv=14.5

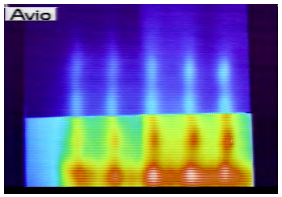

C: Rv=15.5

Infrared beamlet images with different Rv

- The extraction voltage is applied between PG and EG, and the acceleration voltage is applied between EG and MSGG. EG and SG are electrically connected.
- The beam width obtained at calorimeter changes as a function of voltage ratio of acceleration voltage to extraction voltage (Rv = Vacc/Vext).
- Infrared beamlet images are shown on the right hand side of above figures at the voltage ratios of 13.5, 14.5 and 15.5.

Analysis of Infrared Beamlet Images

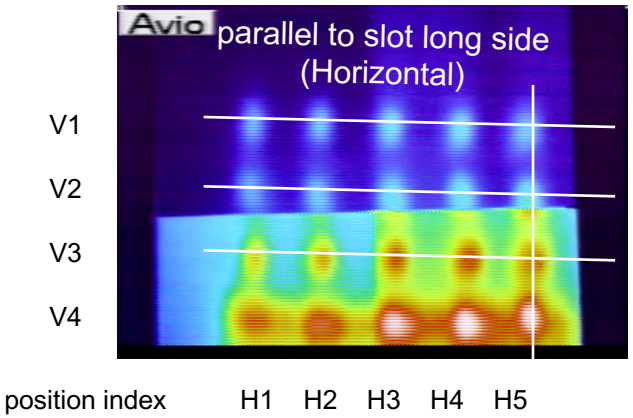

Infrared beamlet images.
Horizontal direction is parallel
to slot long side of grounded grid.

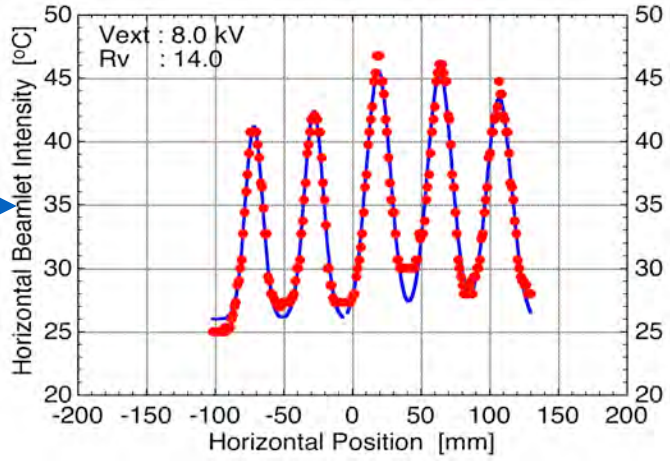

Digitization of IR image and curve
fitting with Gaussians

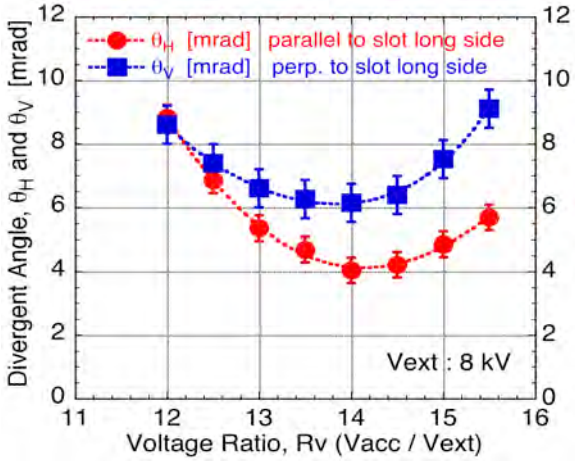

Horizontal and vertical beamlet widths
In terms of voltage ratio (Rv=Vacc/Vext)

- 2-dimensional infrared beamlet images are converted numeric matrix data.
- The numeric data are fit with Gaussian functions, and 2-dimensional e-folding half widths are obtained from the data.
- Horizontal and vertical beamlet divergent angles change as a function of voltage ratio of acceleration voltage to extraction voltage (Rv = Vacc/Vext).
- Minimal beamlet divergences:

  Horizontal direction : 4.1 mrad,

  Vertical direction : 6.1 mrad

Status of negative-ion-based LHD NBI (H^- case)

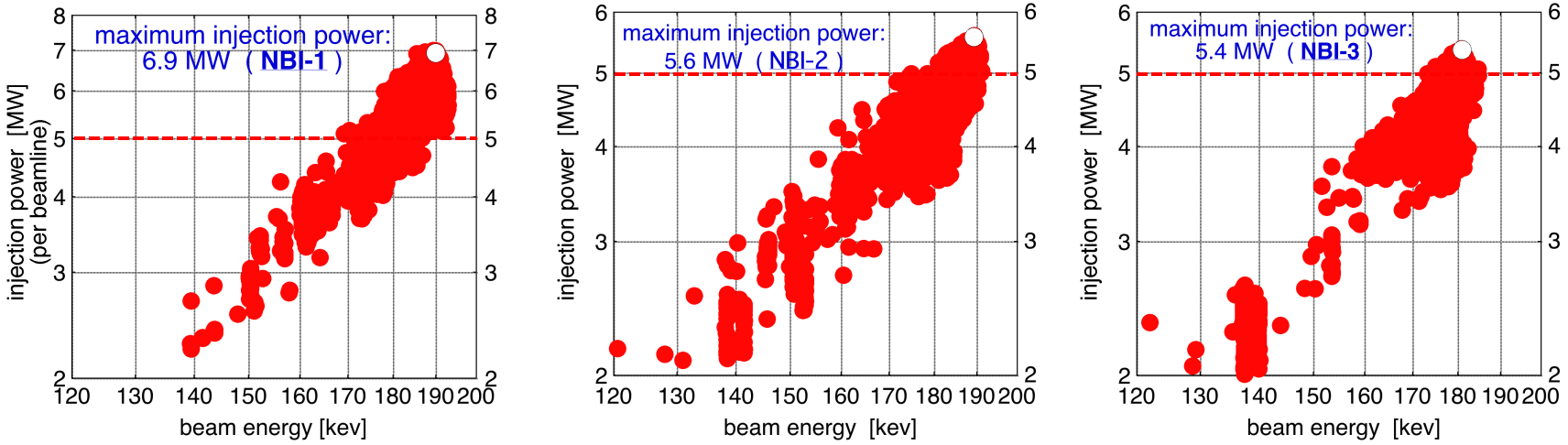

- Each negative-ion-based NBI achieved the nominal injection power of 5 MW.

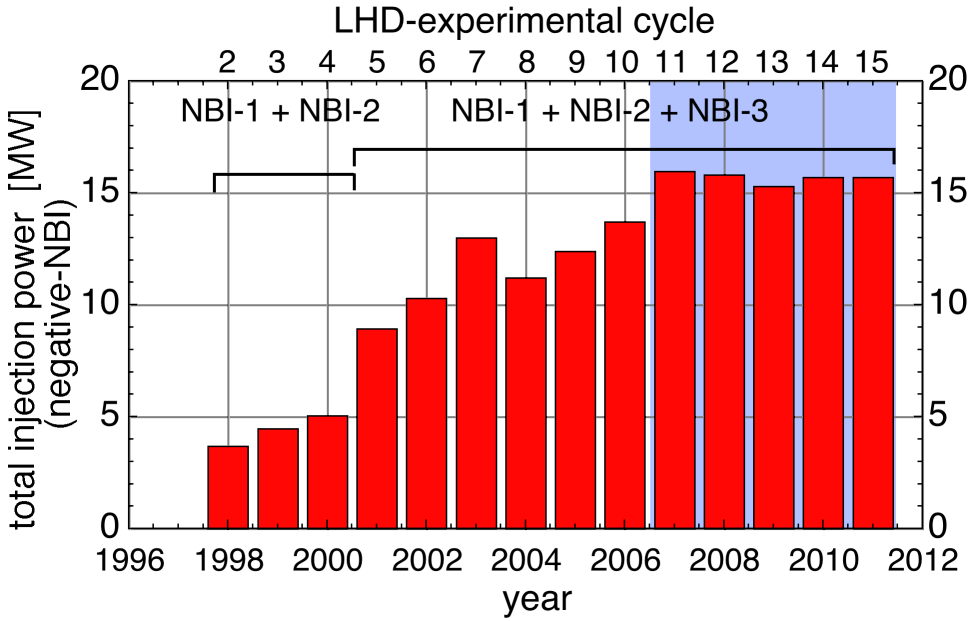

- Total Injection power with all the negative injectors reaches 16 MW in 2007 and has been kept above 15 MW since 2007.

Physics Study of Source Plasmas and Beams

Production and Transport Mechanism of H^-/D^-

1. Improvement for ion sources
   - Enhancement of H^- / D^- current in high power injection.
   - Improvement for the beam uniformity on whole the electrode. Wide-area perveance matching and reduction of co-extracted electrons.
2. Mechanism of H^- / D^- production in ion sources
   - What is the parent particle of H^- / D^-? H^+ / H^o (D^+ / D^o)
   - Density distribution of the positive and negative ions, electron and neutral particles in the beam extraction region.
3. Transport and extraction mechanism of H^- / D^-
   - Does meniscus exist in the Cs seeding condition?
   - Potential structure and distribution of charged particles in the beam extraction region.

Ion source plasma is controlled with the structure and strength of magnetic fields

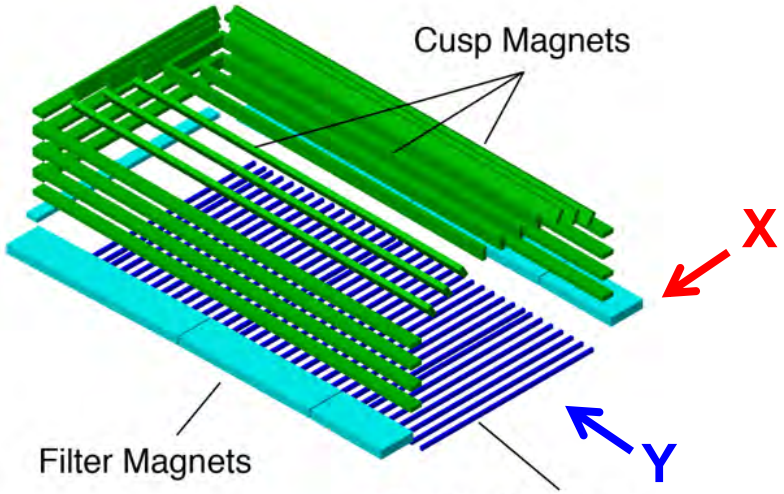

Magnet configuration

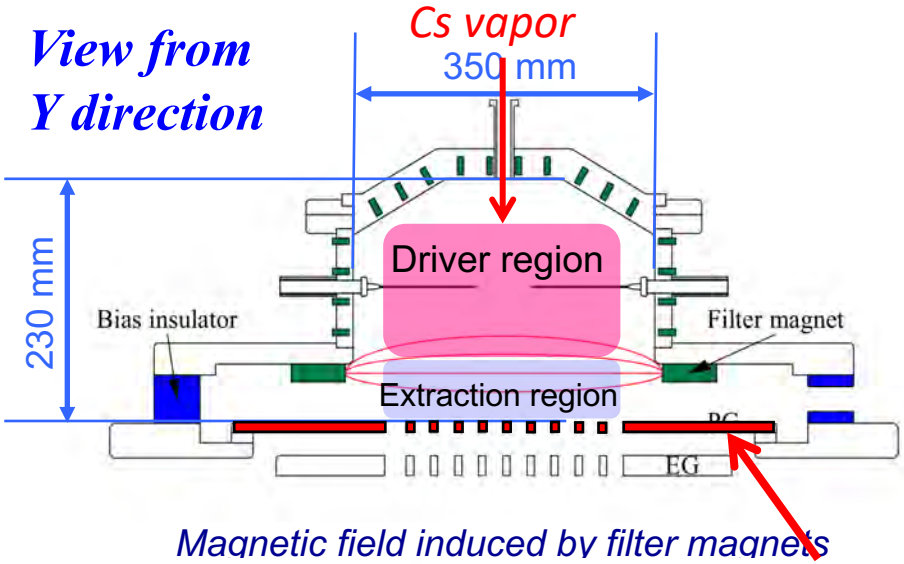

Magnetic field induced by filter magnets

- *Driver region and beam extraction region:*
  - *Driver region*: Filament-arc plasma (hot electrons) Dense plasma is confined with cusp magnetic field.
  - *Extraction region*: Diffused plasma Magnetic filter field reduces the plasma density and electron temperature < 1eV.
- *H^- ions are produced on the plasma grid (PG)*
- ***Electron deflection field plays an important role in negative ion sources.***

Plasma grid (PG)

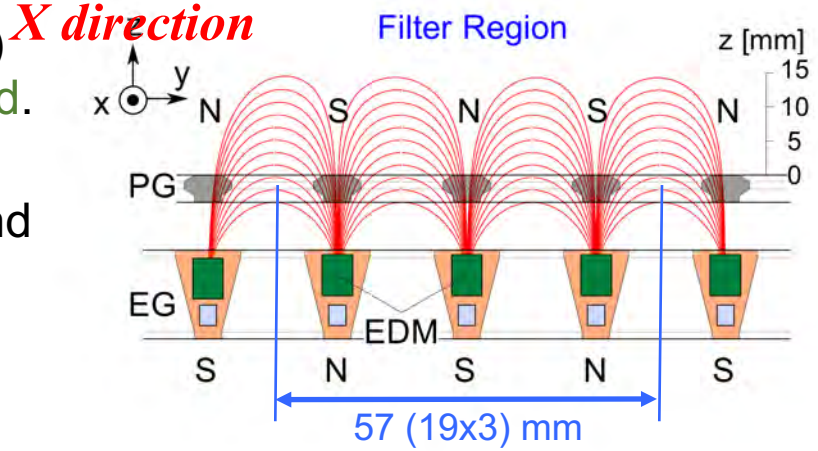

Magnetic field induced by electron-deflection magnets

Plasma diagnostics in a NIFS negative ion source

- Filament-arc source with a pair of filter magnets.
- Size of arc chamber: 350 (W) x 230 (D) x 700 (H) in mm.
- Diagnostic modules are installed on the bias insulator with 52 mm thick.

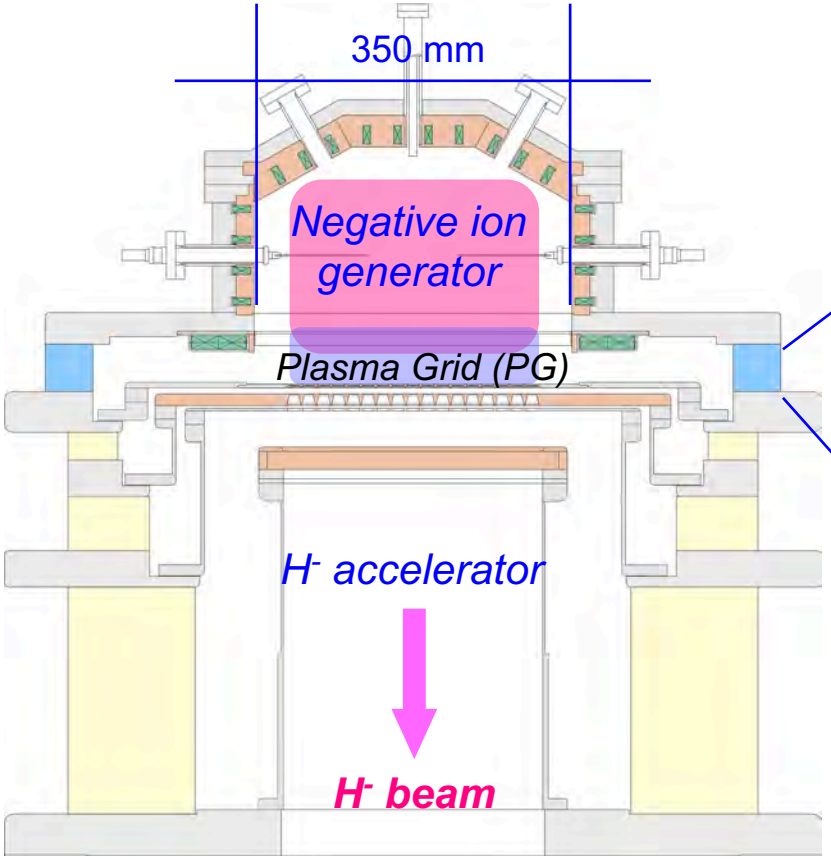

Cross-section of NIFS-RNIS

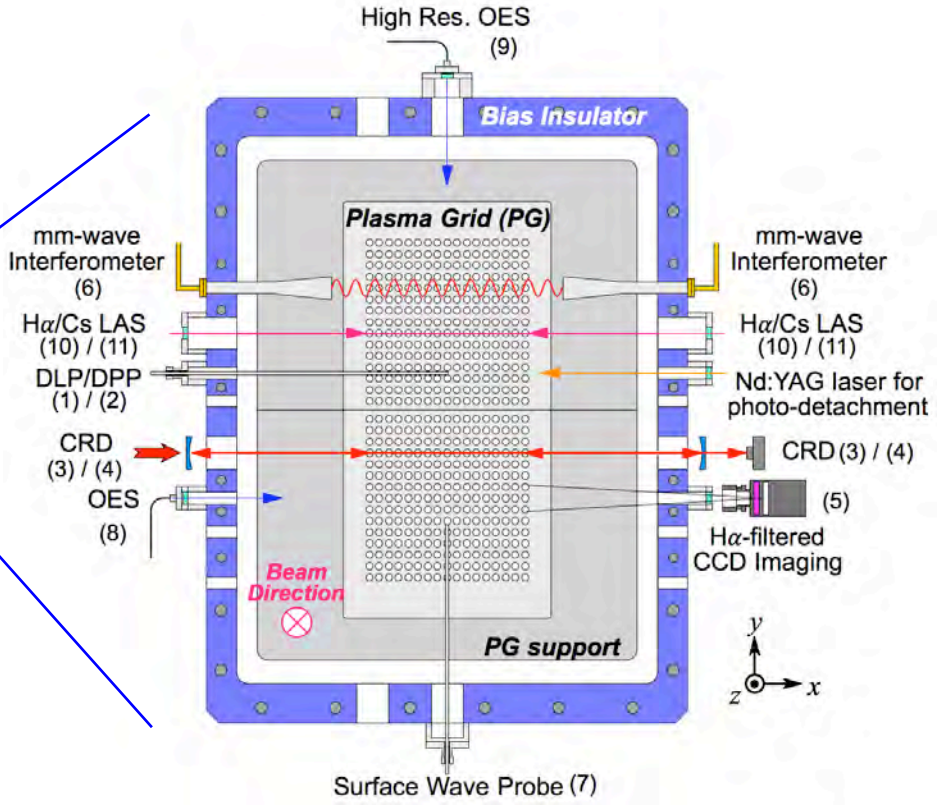

Arrangement of diagnostic system viewing from back-plate side

Formation of Negative-Ion plasma in Cs seeded plasma

Decrease of electron due to Cs seeding

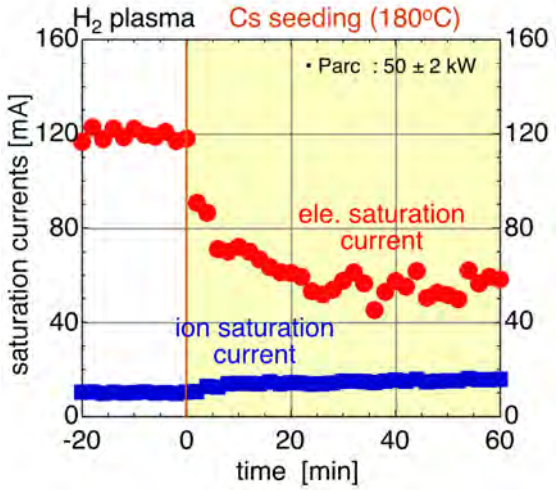

Changes in probe V-I curve

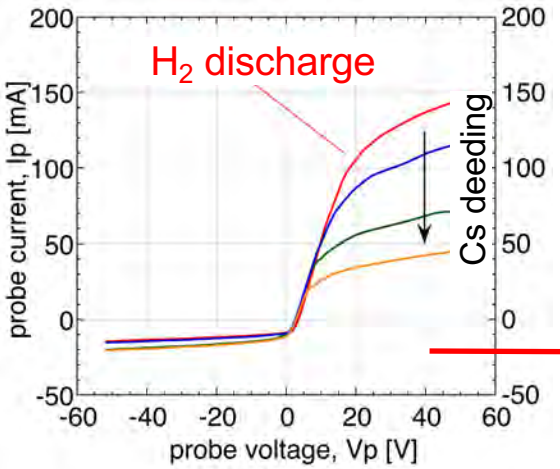

positive-ion negative-ion plasma

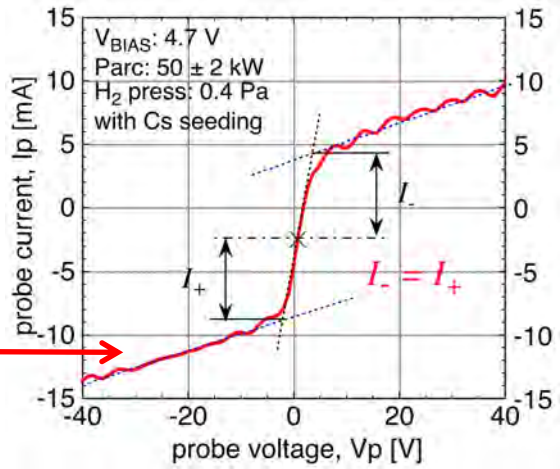

- before Cs seeding

  positive ion : electron ≈ 1 : 10 (at 9 mm apart from PG)

- after Cs seeding

  - symmetric V-I characteristic
  - quite low electron density
  - (positive ion) : (negative ion) ≈ 1 : 1

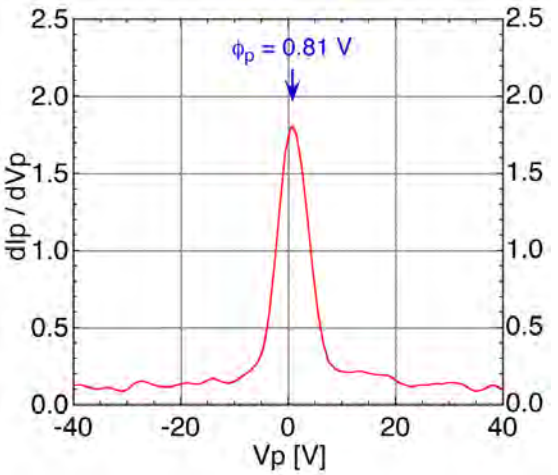

- "*electron*" saturation current → "*negative*" saturation current, I_-.
- "*ion*" saturation current → "*positive*" saturation current, I_+.

Negative saturation current increases by applying beam extraction field

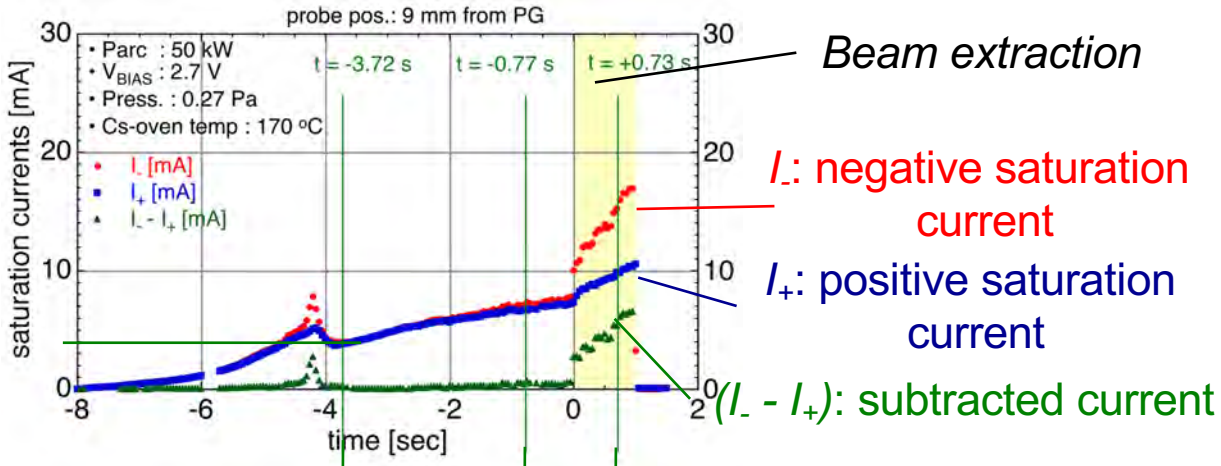

Pre-arc period

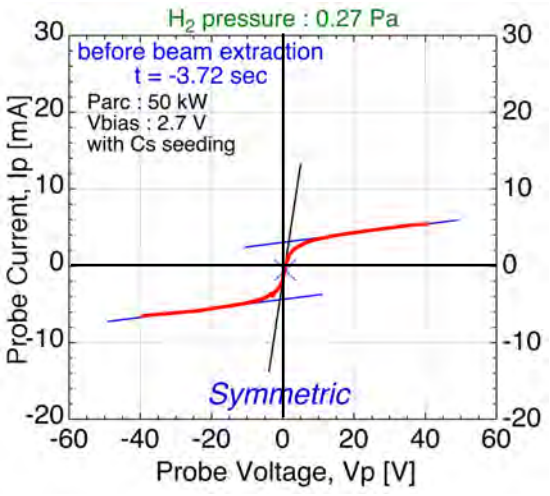

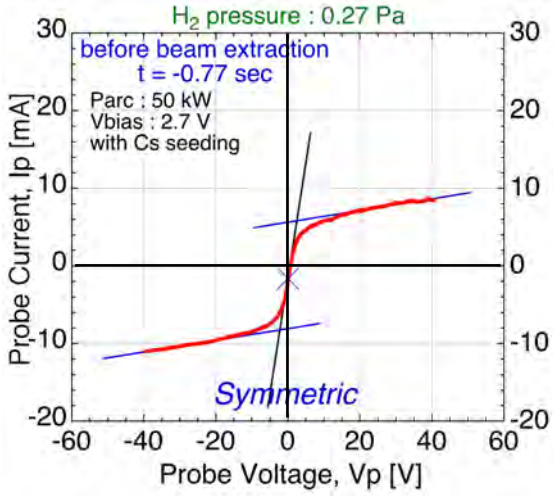

Beam extraction

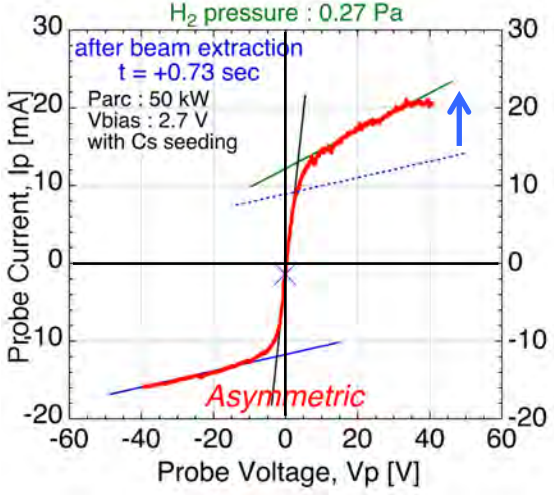

Response of Negative-Ion Plasma to External Electric Field

Waveform of H^- density
(Photodetachment signal)

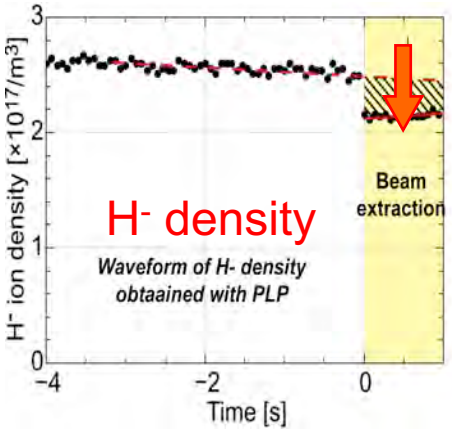

Waveform of negative saturation current
(Langmuir-probe signal)

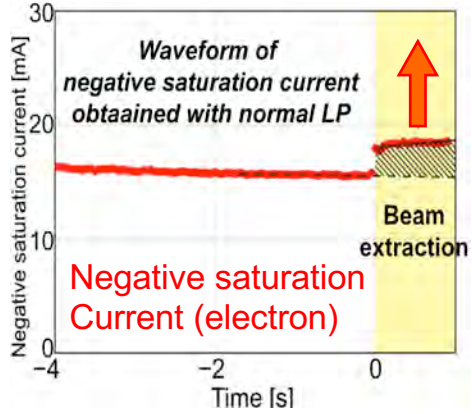

Electron compensates for extracted H^- ion density

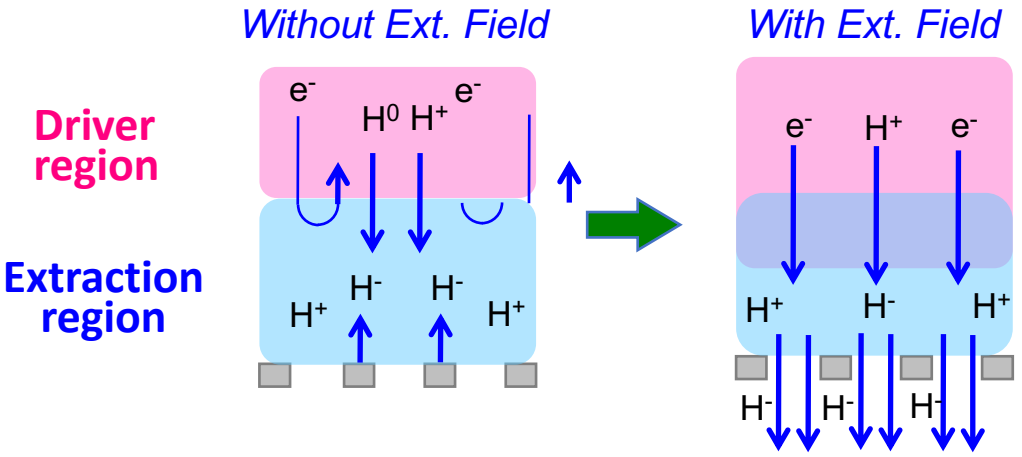

- Without extraction field, the charge neutrality is kept by H^- and positive ions in the beam extraction region.
- By applying extraction field, H^- density decreases in extraction region.
- To conserve the charge neutrality, electrons move from electron-rich driver region.

Formation of negative-ion plasma

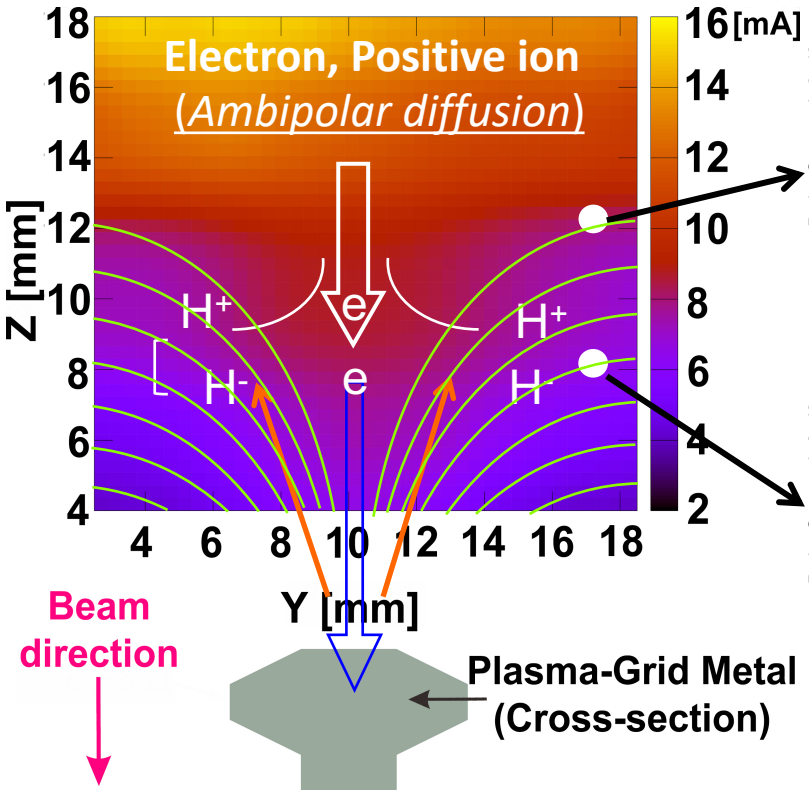

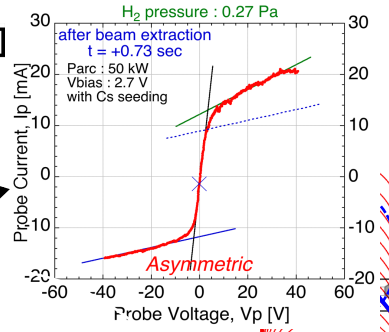

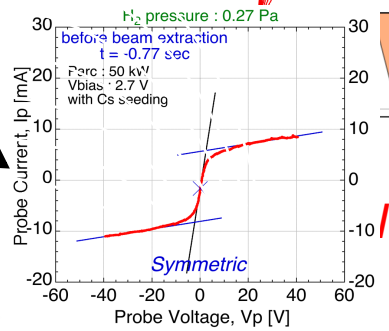

Above metal part of PG, negative-ion plasma includes more electrons.

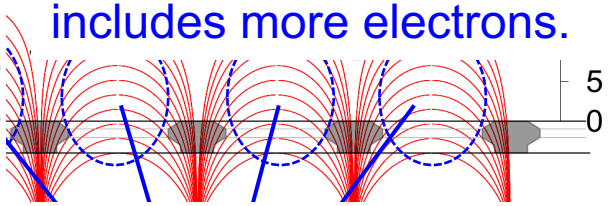

On the other hand, very low density of electron observed in the negative ion plasma above PG apertures.

Electrons have smaller gyro radii.
→ They are absorbed partially in the metal part of plasma grid.
→ Electrons are filtered by the outer loops of electron deflection magnets.

Positive ions (H^+, H_2^+, H_3^+) have larger gyro radii than electrons.
→ They cannot penetrate inside plasma grid.
→ Converted H^- ions have larger gyro radii then electrons, and possible form negative-ion plasma inside EDM loops.

S. Geng et al., Plasma Fusion Res. ***10****, 3405016 (2015)*

Where are the negative ions extracted?

Schematic view of
the setup of Hα-filtered CCD

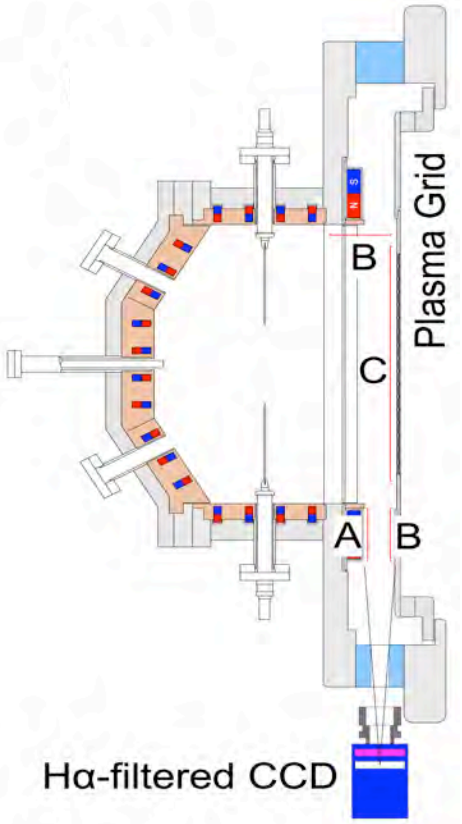

View taken w/o plasma

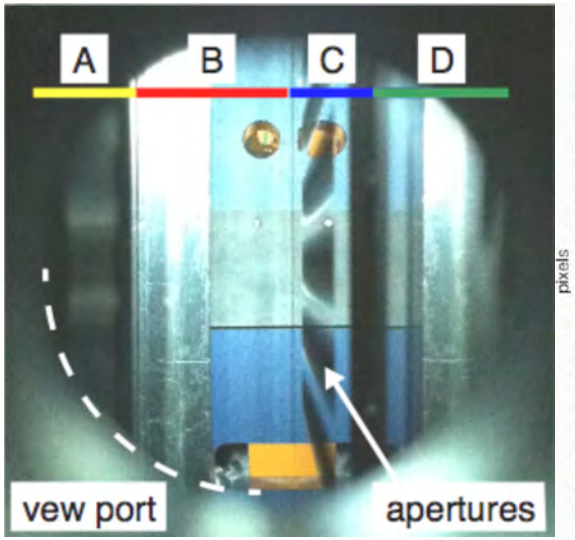

Subtracted CCD image,
during and before extraction

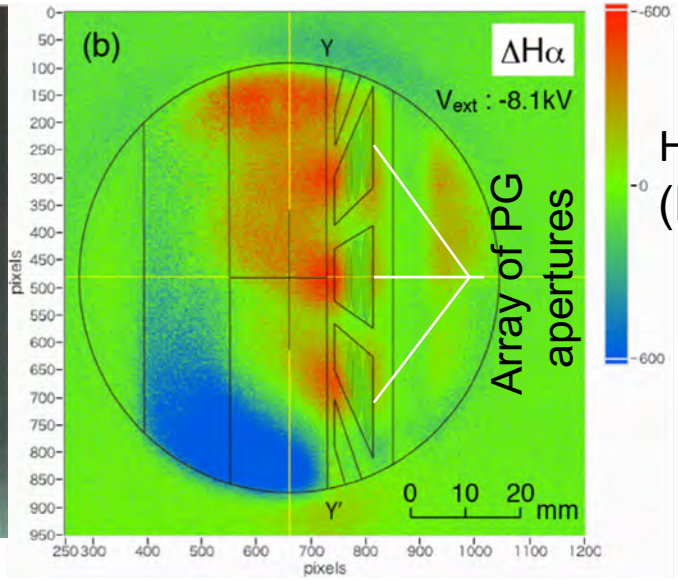

Decrease

Hα intensity
(H^- density)

Increase

Distribution of extracted H^- ions localized mainly in the electron deflection field penetrated inside source plasma.

K. Ikeda et al., New J. Phys. ***15*** *(2013) 103026*

Directional Photodetachment Langmuir Probe (DPLP)

Directional Photodetachment Langmuir Probe (DPLP)

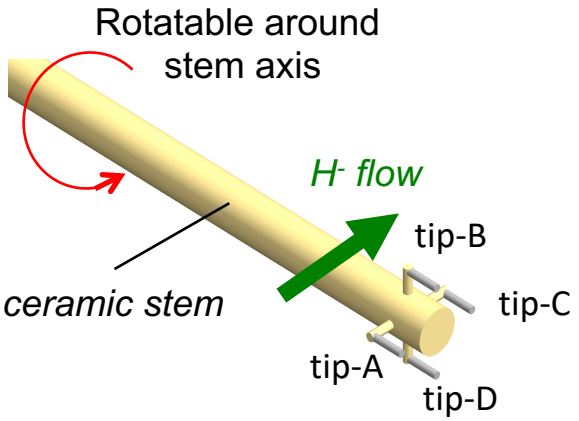

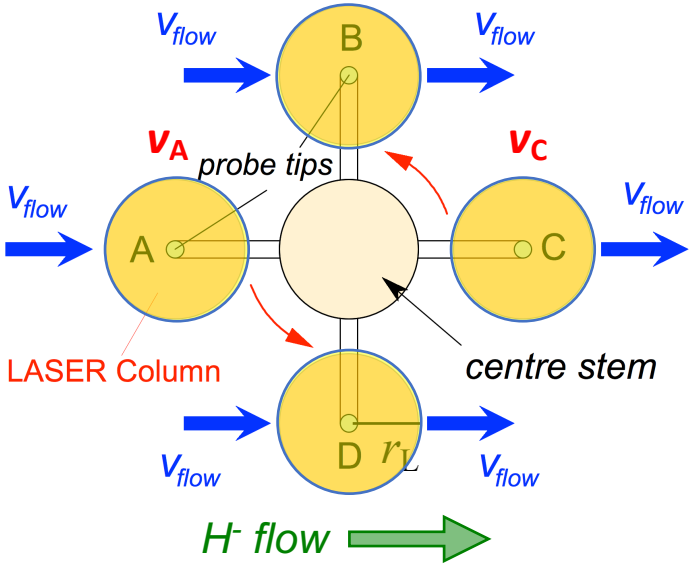

$v_{flow} = (v_A - v_c) / 2$

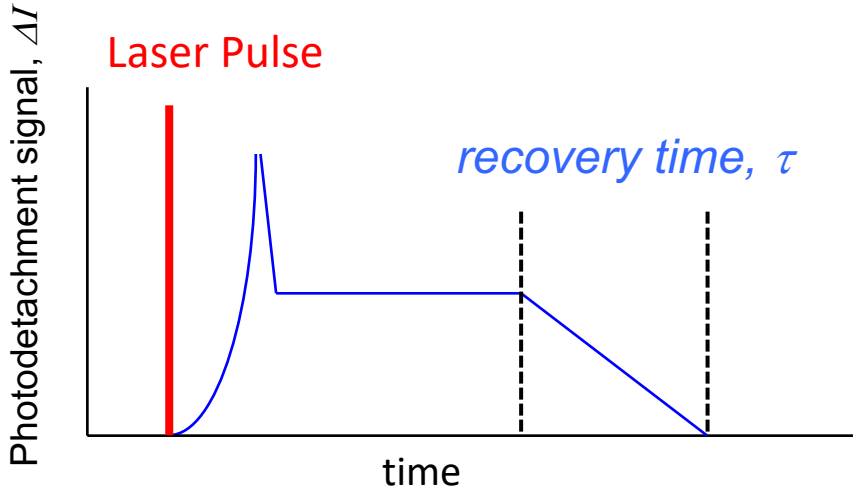

S. Geng et al., Rev. Sci. Instrum. ***87*** *(2016) 02B103*

Using a shade of center stem, flow velocity of H^- ions is enable to estimate.

The velocity at each probe tip is evaluated by r_L / τ, where r_L and τ are radius of laser column and recovery time, respectively.

Negative ion flow

S. Geng et al., Fusion Eng. Des.,
http://doi.org/10.1016/j.fusengdes.2017.02.041.

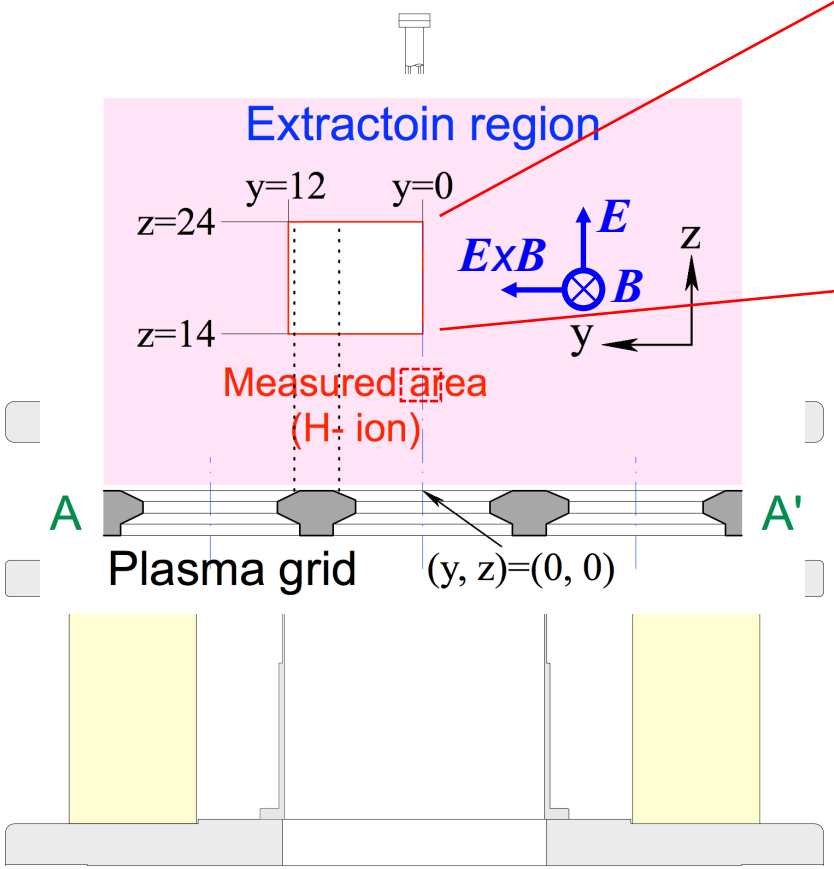

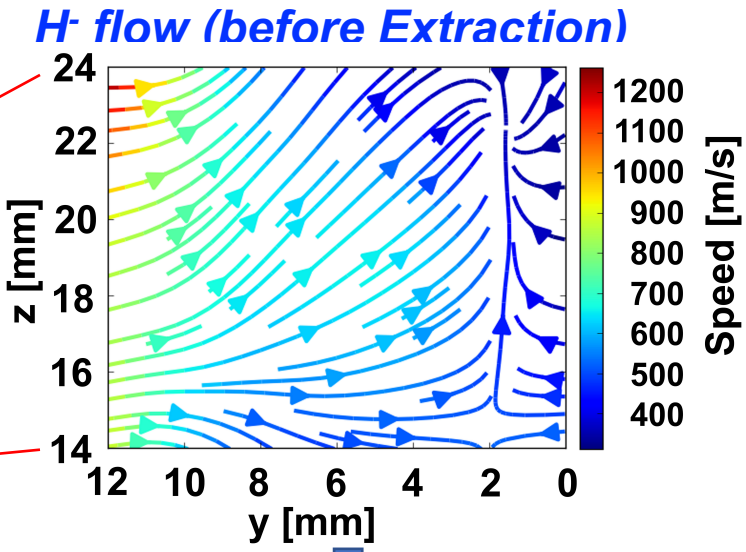

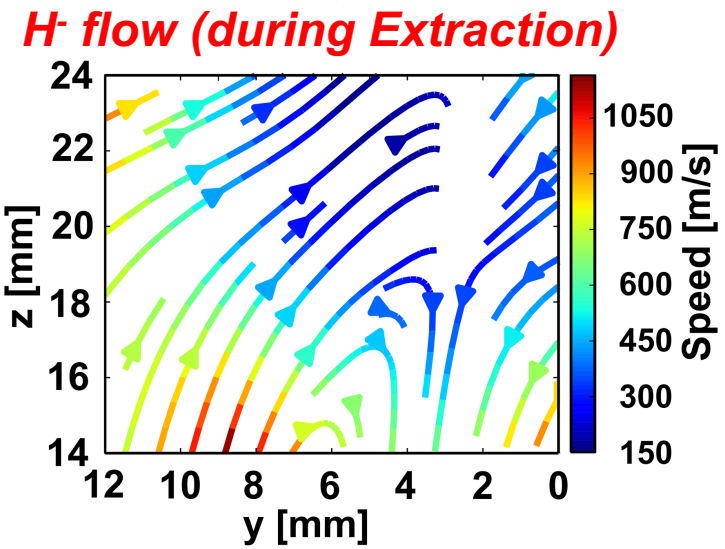

Injection from Hydrogen to Deuterium Beams

From Hydrogen to Deuterium Beams

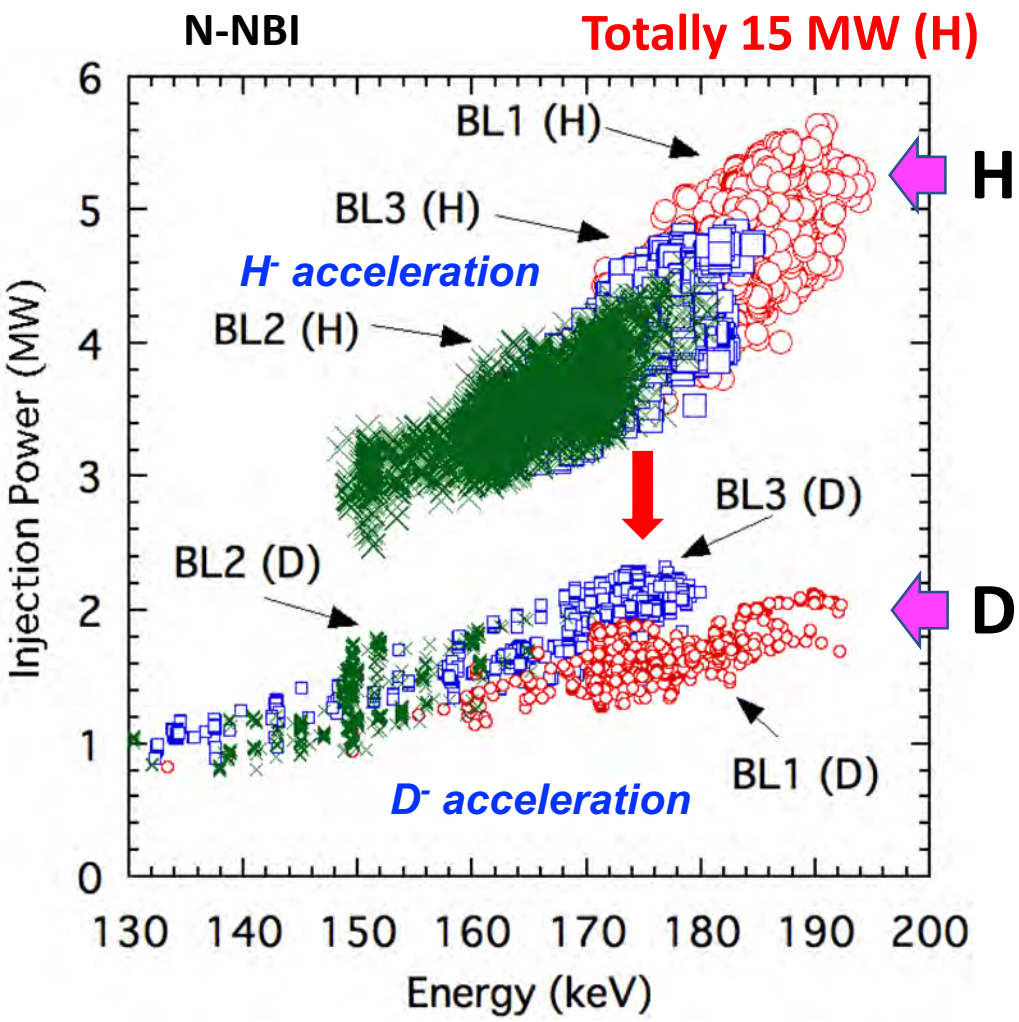

Beam injection Power with respect to input arc power in H^- and D^- operations

H^- acceleration

H	I_e / I_{H^-}	Energy	Inj. power
BL1	0.27	190 keV	**5.6 MW**
BL2	0.30	178 keV	**4.6 MW**
BL3	0.23	185 keV	**4.8 MW**

D^- acceleration

D	I_e / I_{D^-}	Energy	Inj. power
BL1	0.49	190 keV	**2.1 MW**
BL2	0.54	171 keV	**1.9 MW**
BL3	0.39	178 keV	**2.3 MW**

K. Ikeda et al., Nucl. Fusion 59 (2018) 076009.

Measurement of the source plasmas (H and D)

Densities of negative ions, positive ions, electron and plasma potential were measured in NIFS NBI teststand.

Discharge gas was changed from H_2 to D_2.

Density of D^- ions increased 1.3 times lager than that of H^-.

Density of electrons increased much higher, ~3 times, in the D_2 discharge.

Higher transport of deuterium plasma lead to the higher electron current

H. Nakano et al., OR17AM-C04 (this conference)
M. Kisaki et al., PO18AM-025 (this conference)

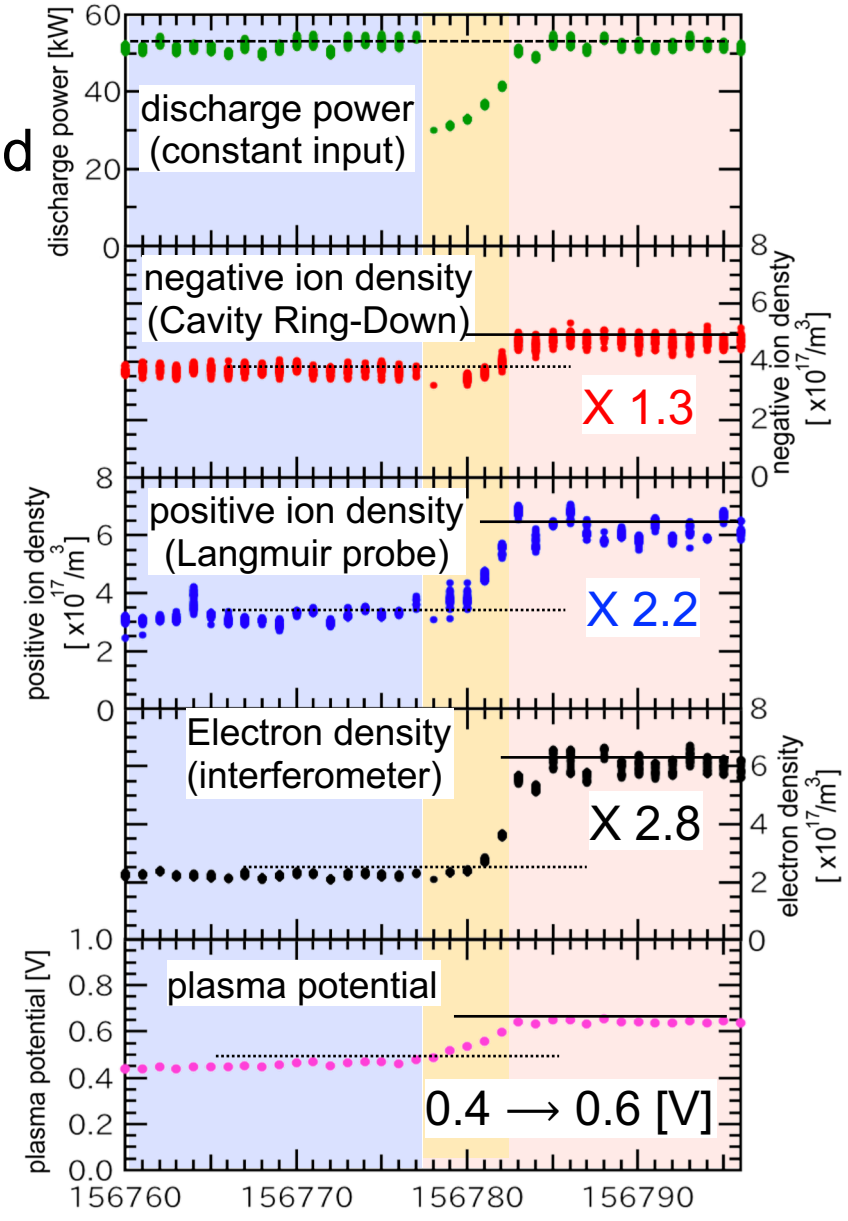

What is the key point?

At moving the acceleration from H^- to D^- beams, the following changes appeared;

1. Increase of co-extracted electron current.
2. Decrease of negative ion current.
3. Increase of Cs consumption.

Higher electron current possible to damage the accelerator electrodes.

→Cannot increase the discharge power to increase D^- ions and to increase the beam power.

Electron density increases simultaneously.

Electron suppression inside the ion-source plasma is essential !

Changes in the acceleration from H^- to D^- Beams

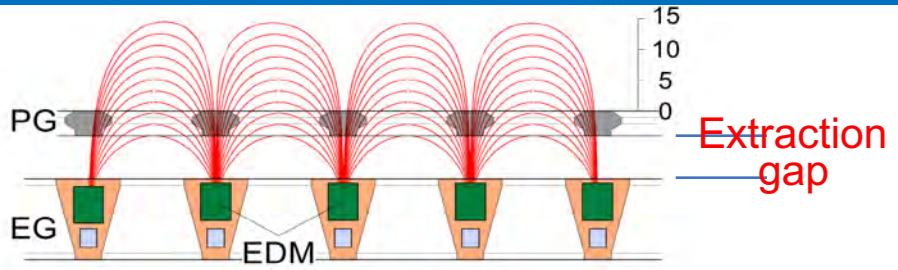

By decreasing the extraction gap, electron deflection field penetrates deeper inside ion source plasma and becomes stronger.

extraction gap: 8 mm

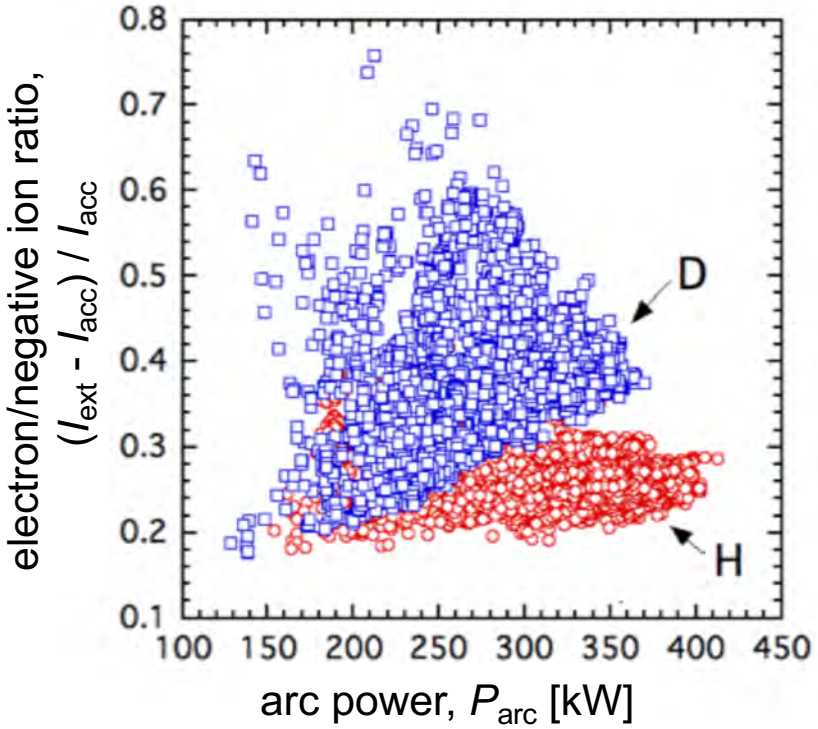

extraction gap: 7 mm

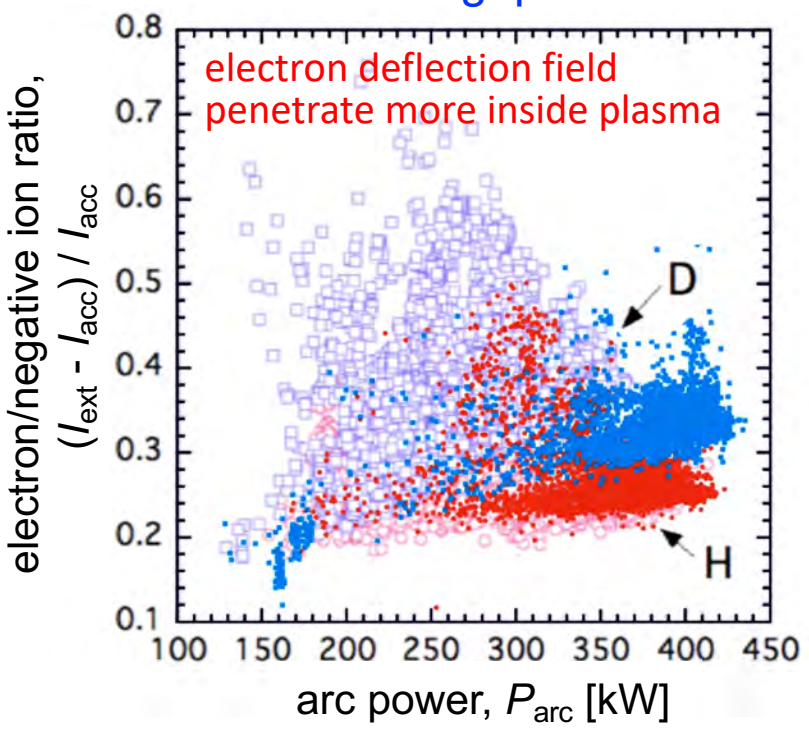

This result suggests that enhancement of the magnetic field near plasma grid is effective to reduce the density of electrons.

Result with Egg Box Cell

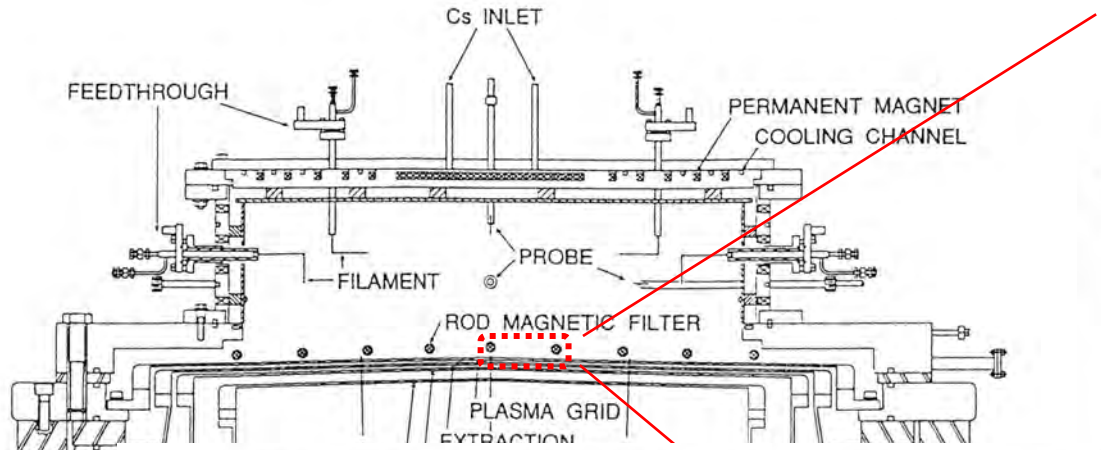

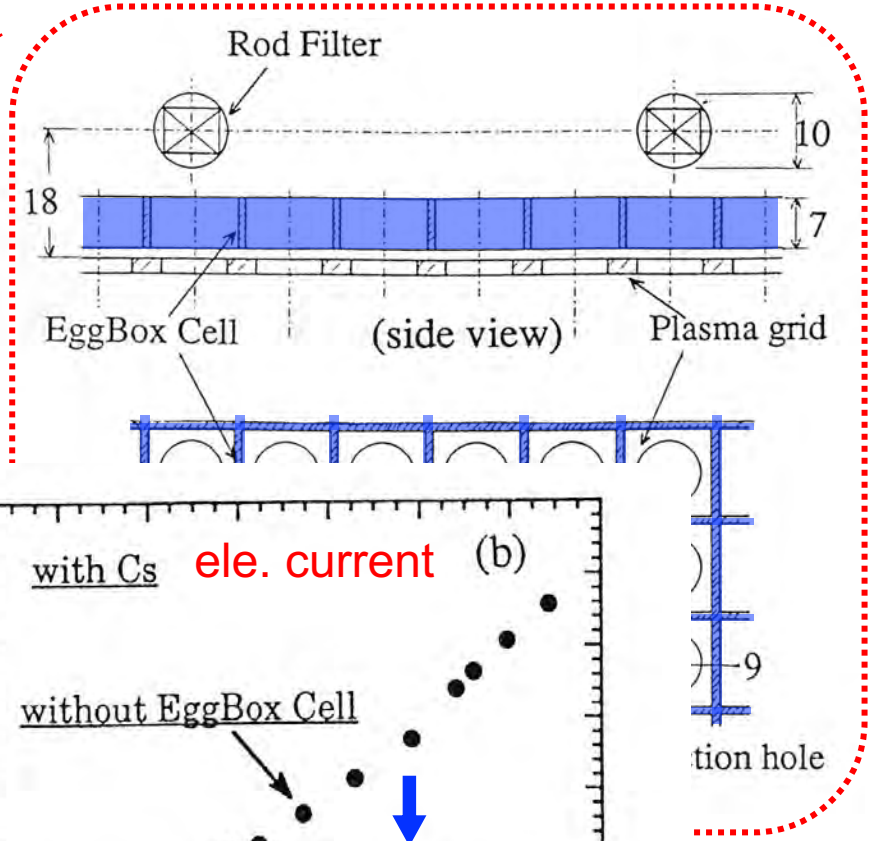

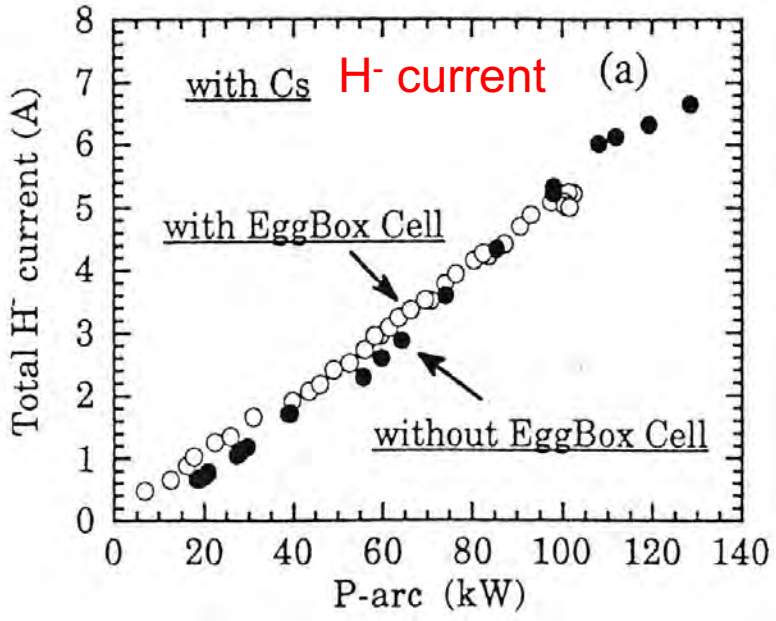

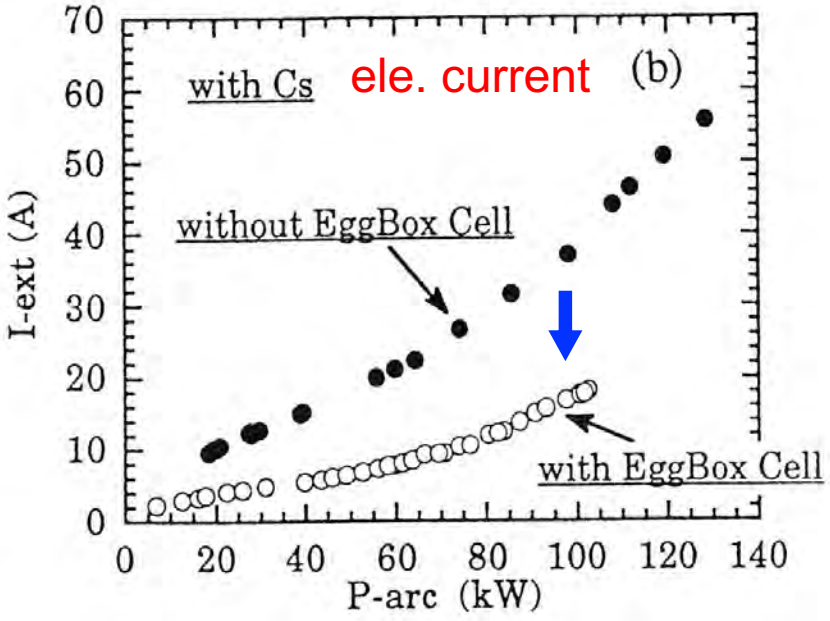

Electron Fence (EF)

Cross-sectional view of LHD ion source

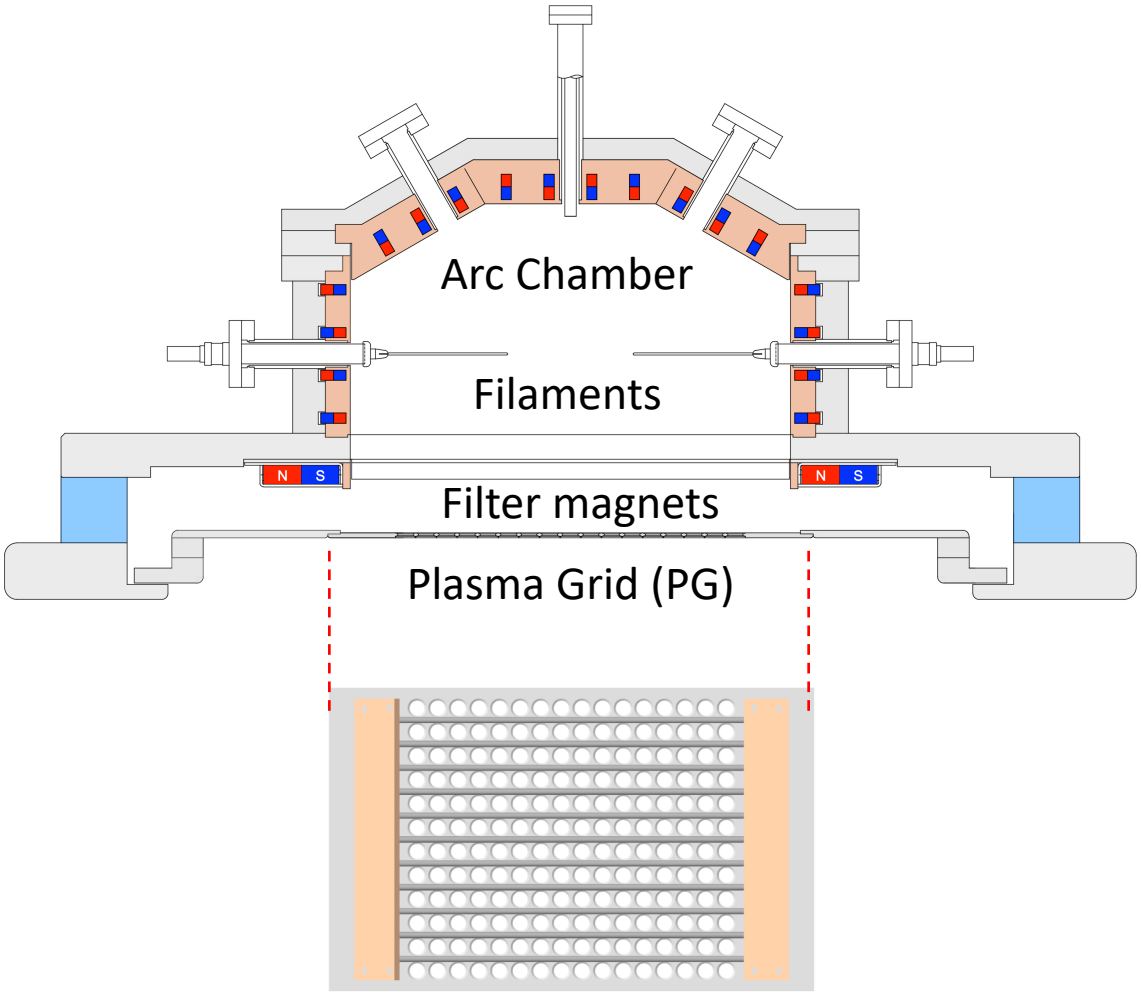

Electron Fence (EF) installed on PG

Electron Fence is made of parallel ϕ5 Mo rods

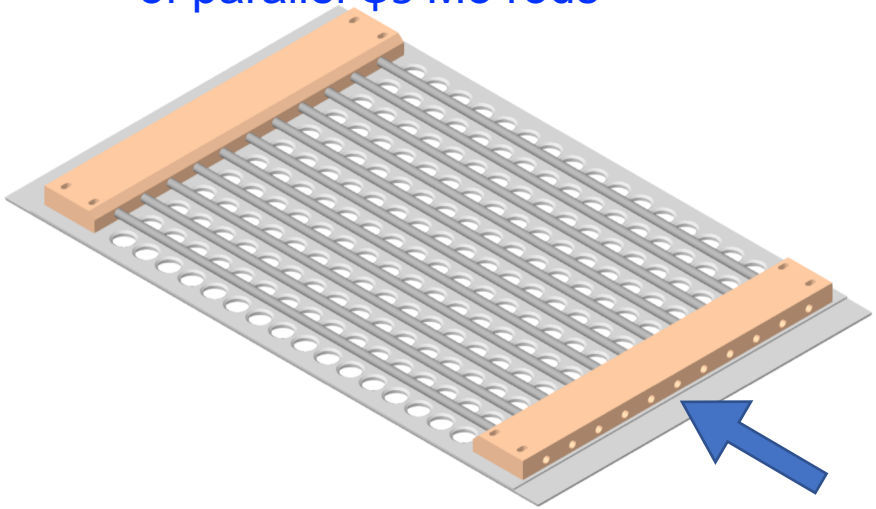

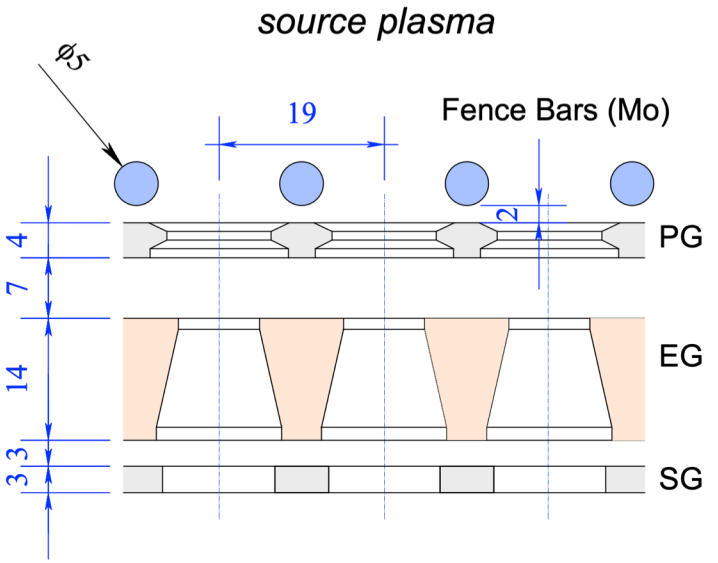

Magnetic field lines are cut with Electron Fence

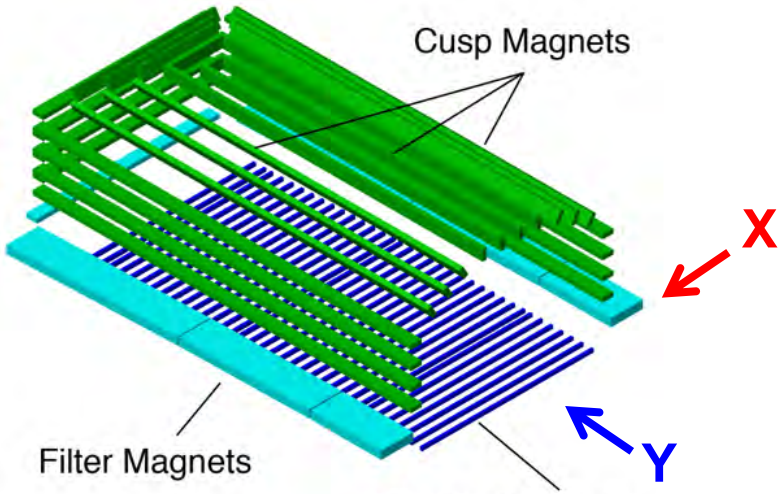

Magnet configuration

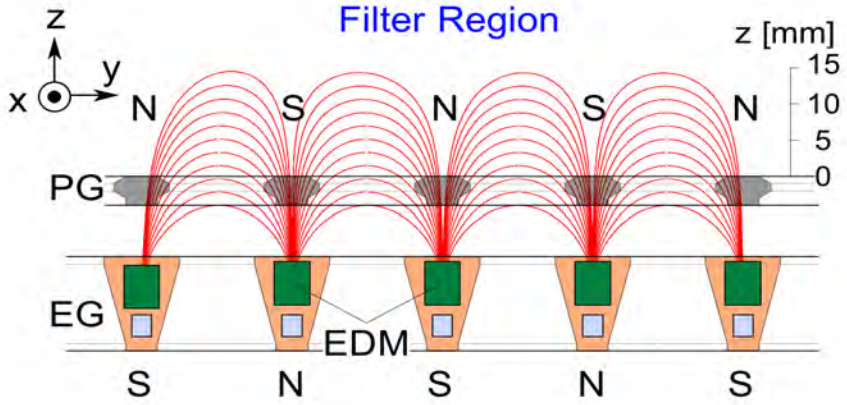

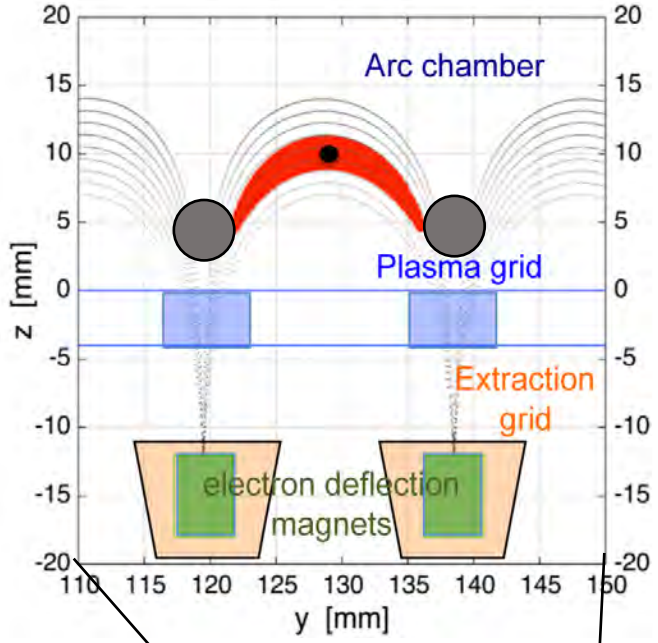

E_e: 1eV

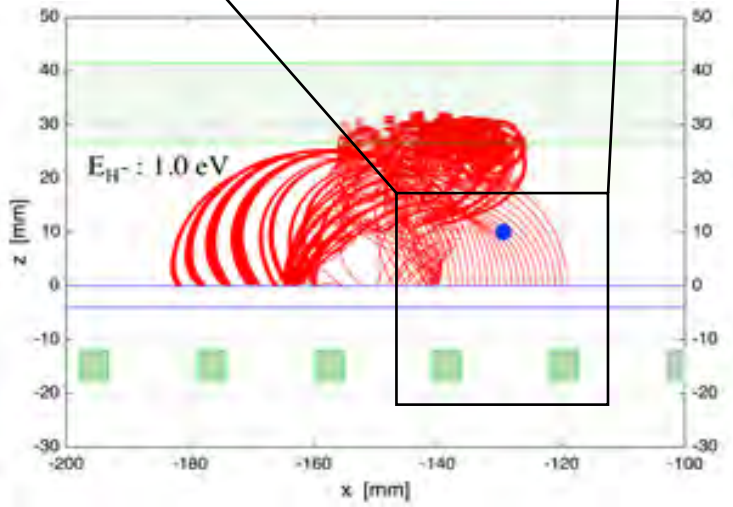

Comparison of time evolutions of H^- and co-extracted electron currents

Trend of original H^- current, I_H-(org), and co-extracted electron current, $I_{co\text{-}ext}$.

[I_H-(org) : I_{acc}
$I_{co\text{-}ext}$: I_{ext} - I_{acc}]

Trend of the ratio of co-extracted electron current, $I_{co\text{-}ext}$, to original H^- current, I_H-(org).

[R_e : (I_{ext} – I_{acc}) / I_{acc}]

with EF(2019)

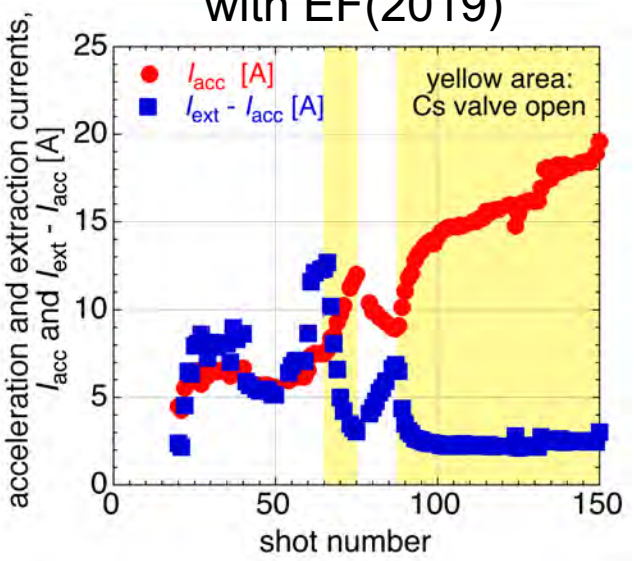

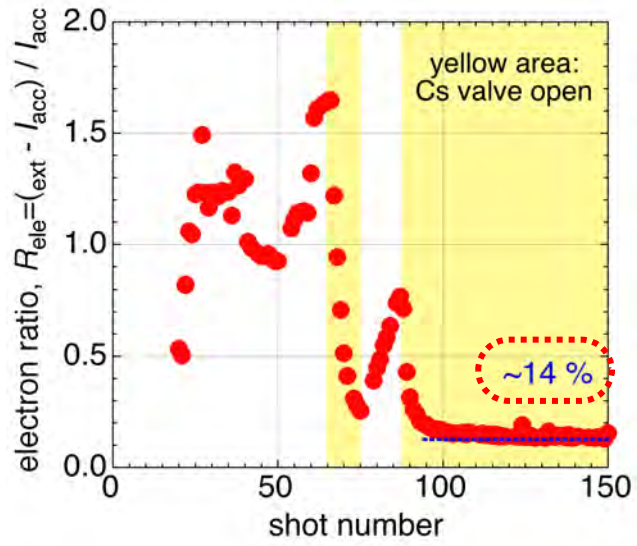

without EF(2018)

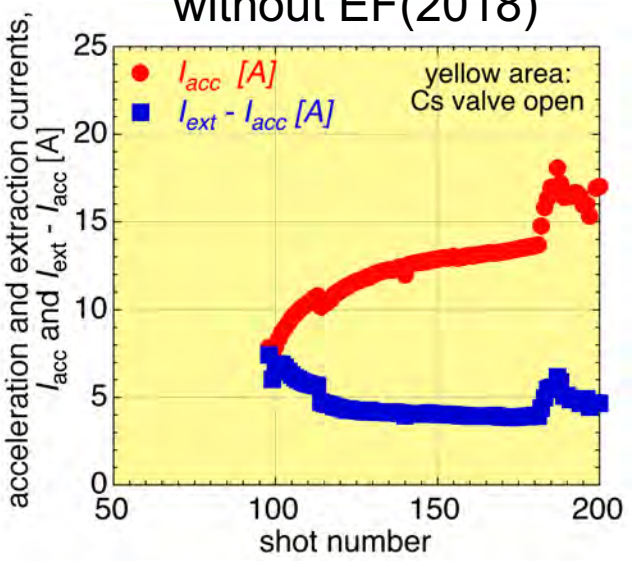

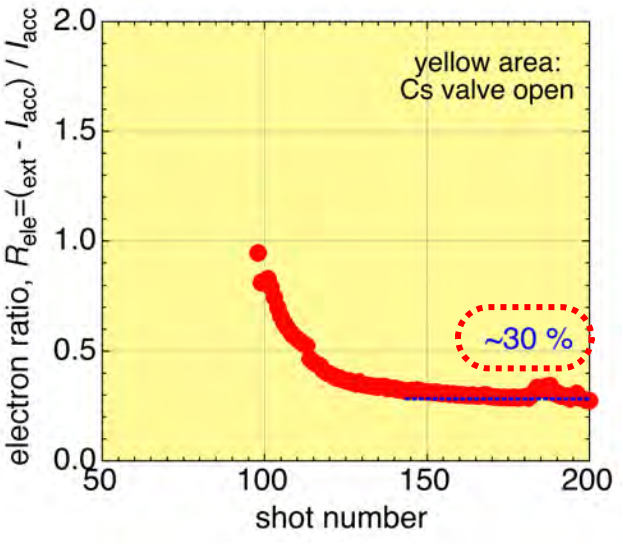

Ratio of co-extracted electron current to H^- current is reduced about a half value with EF.

Summary

- Optimized magnetic configuration, which leads to longer electron life time, is necessary to obtain larger production rate of H^-/D^- ions
- Multi-Slot Grounded Grid (MSGG) with high beam transparency is adopted for high power beam injection.
- Horizontal and vertical focal condition of MSGG has been resolved by applying "racetrack aperture" to steering grid.
- Detailed beam characteristics were investigated with beamlet monitor.
- Total injection power with three n-NBI systems achieved 16 MW by accumulating the results obtained with above investigations.
- Diagnostics study of ion-source plasmas and beams have started to understand the physics of H^-/D^- production, negative-ion transport, meniscus and beam transport.
- Formation of "negative ion plasma" with very low electron density was found at beam extraction region of Cs seeded negative ion source.
- Flow pattern of H^- ions has been obtained using directional photo-detachment probe.
- To solve the issues of D^- beams, optimization for D^- beam has started.

Neutral Beam Injection

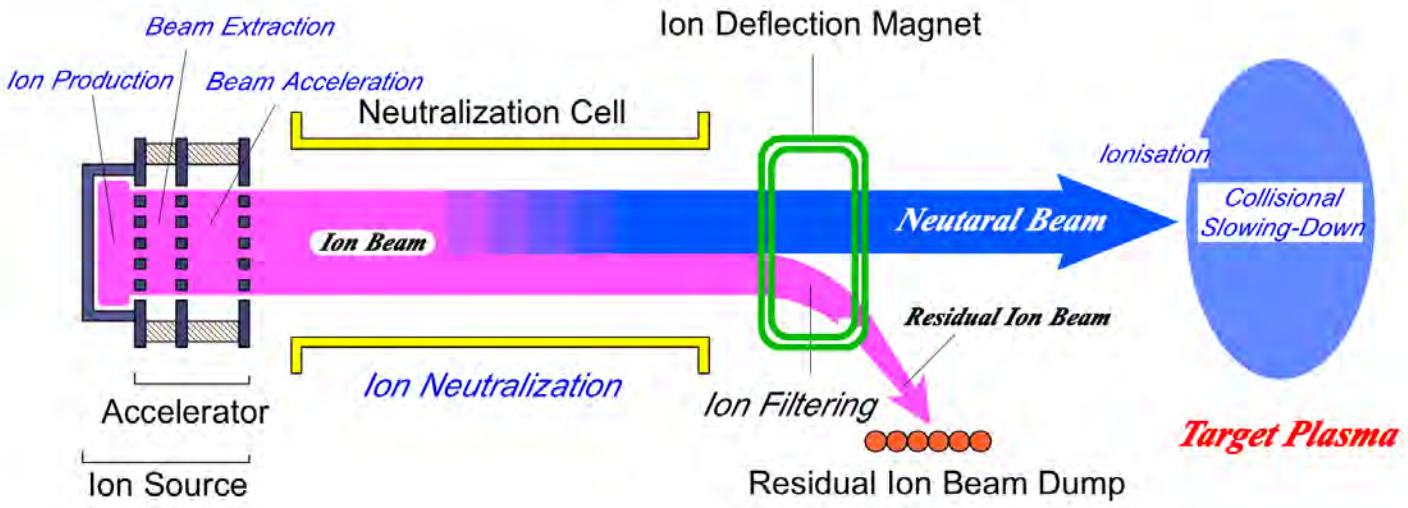

Production of hydrogen ions in ion sources

→ Electrostatic acceleration of the ions (Beam formation)

→ Neutralization of the ion beams

→ Removal of the residual ions using the ion deflection magnet

→ Injection of neutral beam

→ Ionisation

→ Collisional slowing-down

] Inside target plasma

Why negative ion beams are necessary?

- High neutralization efficiency in the beam energy more than 100 keV.
- Beam divergence becomes about 5 mrad at 180 keV by seeding caesium (Cs).

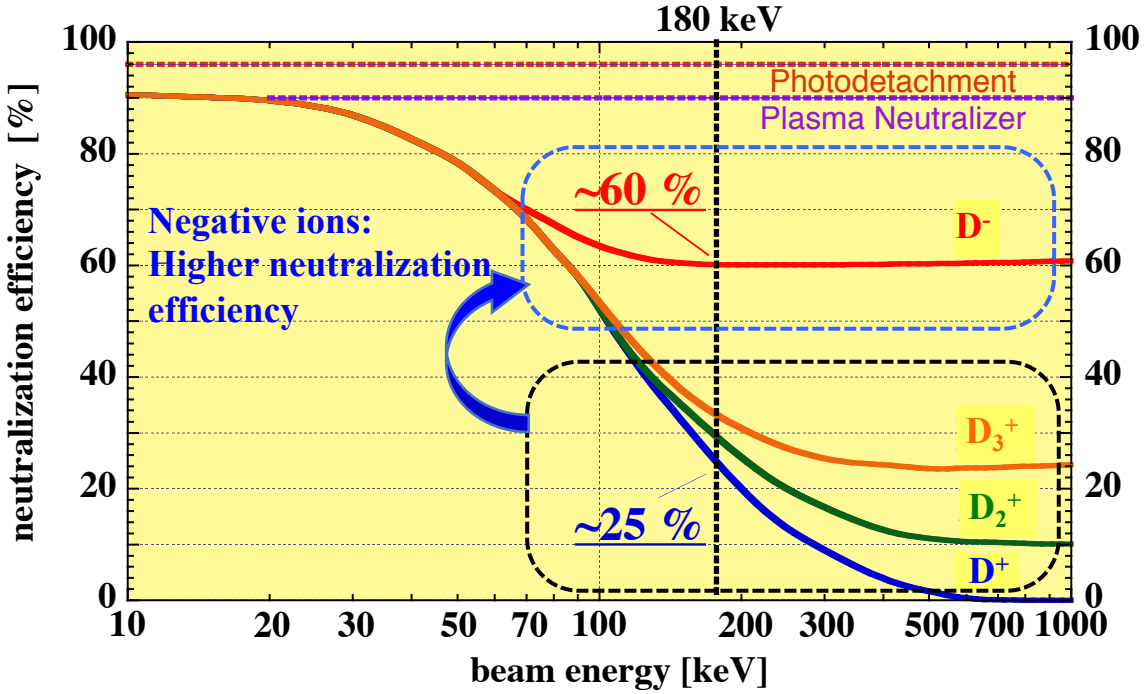

Hydrogen negative ion

- Hydrogen negative ion (H^-) is a two electron system.
- One electron occupies the state close to 1S orbital, and another occupies the orbital with it maximum electron probability at 3.8 times of Bohr radius.

- Additional electron of 1S' orbital trapped at stable "affinity level, ε_A", whose energy level is -0.754 eV from the vacuum level.

  * The vacuum level is the electron of 0 eV without the external field.

Electron Affinities of Some Elements
He: 0.0, Li : 0.62, Be: 0.0, B : 0.28, C : 1.60/1.27
N : 0.07, O : 1.46, F : 3.41, Ne: 0.0 [eV]

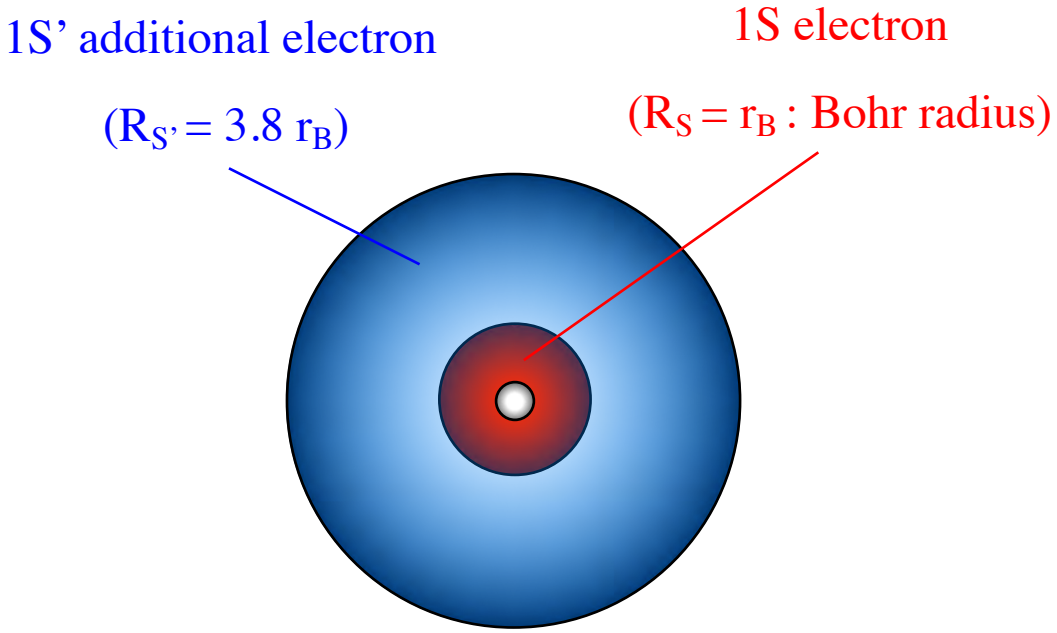

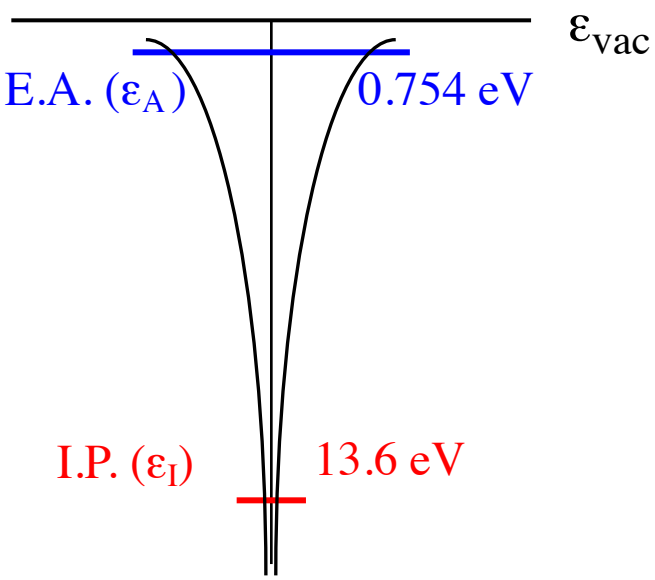

Process of H^- production (volume process)

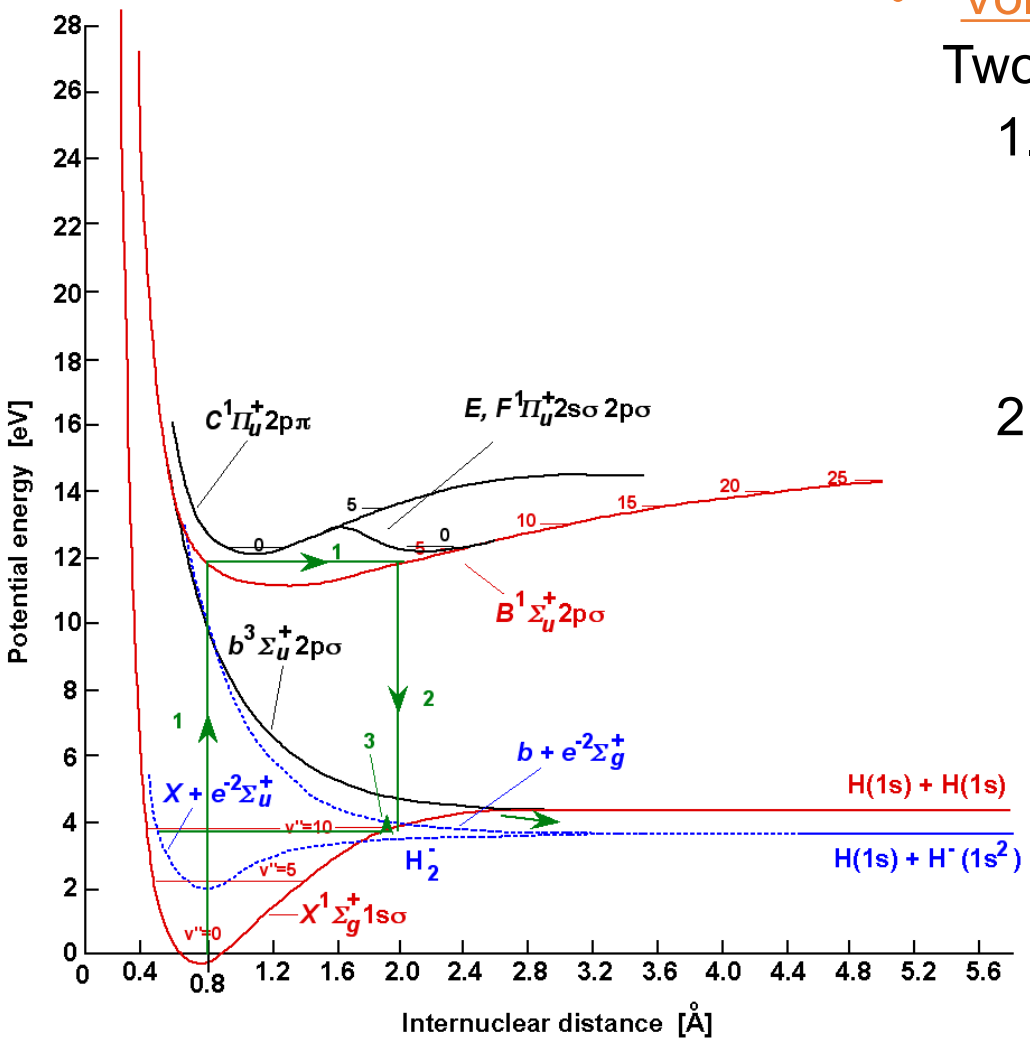

- Volume Production :

  Two-stage electron collisions

  1. H_2 + e (≥ 20eV)

     → H_2^*(excited molecular) + e(fast)

     Vibrational excitation

  2. H_2^*(excited molecular) + e (~ 1eV)

     → H^- + H

     Dissociative attachment

Process of H^- production (surface process)

- Surface Production :

  Electron donation on Cs/Metal surface of low workfunction

  1a. **H_2 + e(>20 eV) → 2H(~2 eV) + e**

  Flank-Condon process

  1b. **H^+ + e (on metal surface) → H**

  Auger neutralization

  2. **H + e (on metal surface) → H^-**

  Resonant transition

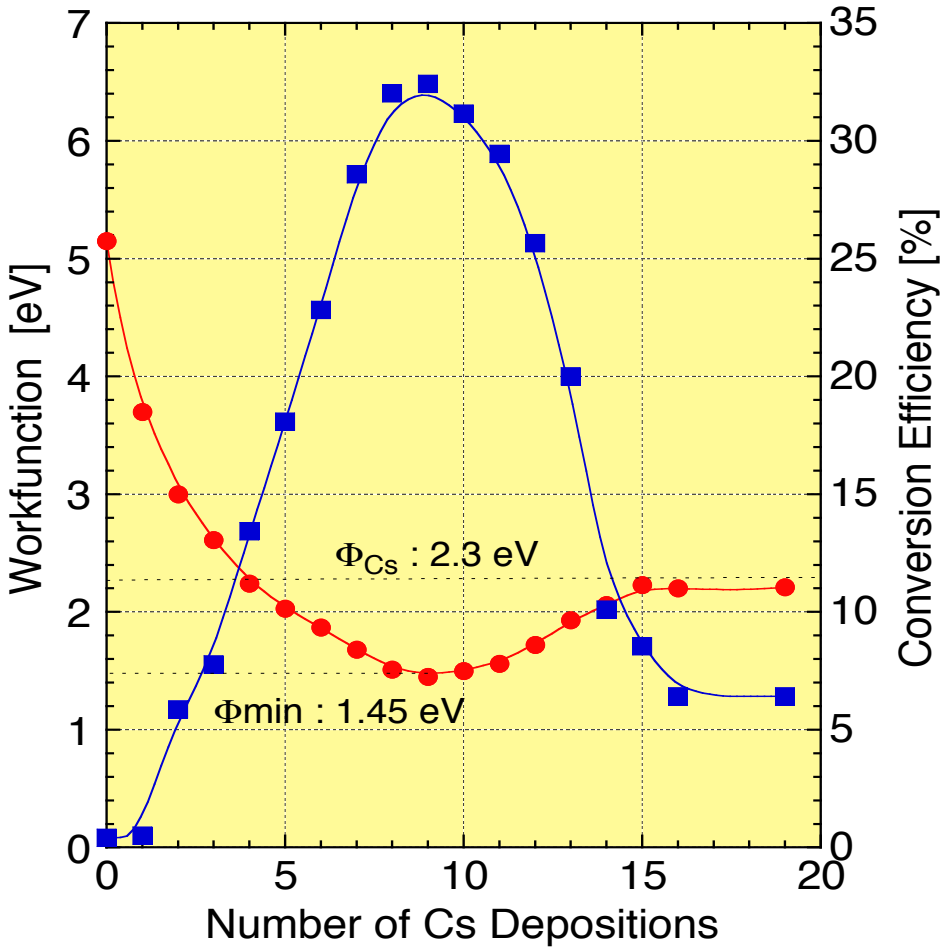

Electron transition on metal surface

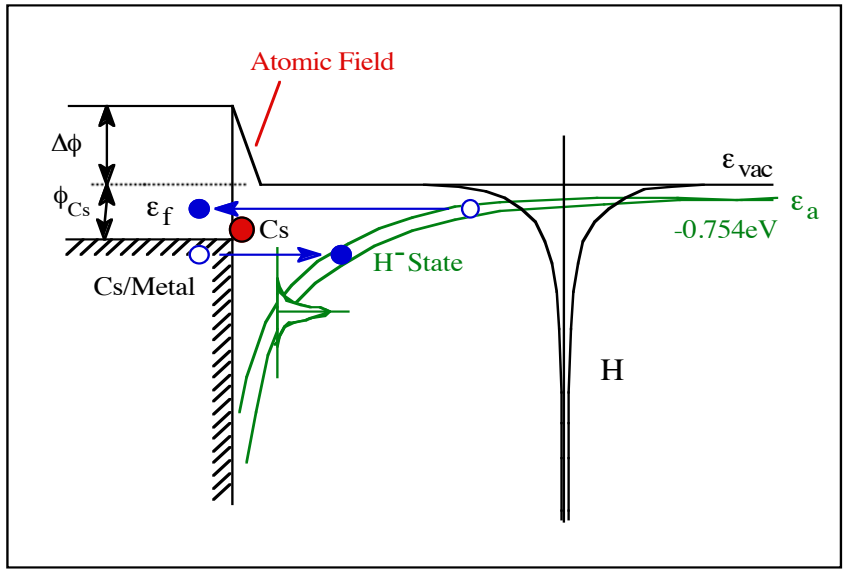

As a hydrogen atom approaches to metal surface • • •

1)The affinity level of hydrogen is lowered by the image potential.

2)The affinity level interacts to electron levels in metal surface and bulk, and the level becomes broad with the width of Δ in below equation.

$$\Delta(x) = 4\pi/h\Sigma\rho(\varepsilon_k)|V_{ak}|^2$$

- In very vicinity of metal surface, bulk electron near Fermi level transits to the broadened affinity level due to the “resonant charge transition”, and H- ion is formed.
- When H^- escapes from the surface, the affinity level rises above Fermi level. The electron at affinity level transits back to metal with a probability of following equation:

$$P(t) = exp(-4\pi\Delta_o e^{-\gamma v t} / h\gamma v)$$

- With adsorption of Cs, energy difference of the affinity and Fermi levels decreases. In such situation, the transition probability is enhanced, and the back-donating is reduced. Consequently, the production rate of H- ions increases.

Issues to be achieved

1. Stable H- production High arc efficiency
   - Longer filament life time
   - Stable cesium operation
2. Plasma and beam uniformity
   - Better beam perveance $\rightarrow$ Less voltage breakdowns at beam accelerator
   - Higher total H^- current
3. High performance beam accelerator
   - Less breakdown in high energy beam acceleration
   - Less beam damages on the accelerator electrode
4. Optimization for beam optics
   - Higher beam transmission
   - Less beam induced damages inside beamline